Stochastic dynamic response of delaminated flexbeam like structures

Priyanka Patil[*,**] , Susmita Naskar[‡], M. T. Vinoda[¶] , Dineshkumar Harursampath[§], P. J. Guruprasad[†]

Department of Aerospace Engineering, Indian Institute of Technology Bombay, Mumbai,Maharashtra,400076, India.
Department of Mechanical Engineering, K.J. Somaiya School of Engineering, Somaiya Vidyavihar University, Mumbai, Maharashtra, 400077, India.
Faculty of Engineering and Physical Sciences, University of Southampton, Southampton, SO16 1BJ, United Kingdom.
Department of Aerospace Engineering, Indian Institute of Science, Bengaluru, Karnataka,560012, India.

Abstract

In this work, the free vibration characteristics of flexbeam like structures, typically used in helicopter main or tail rotor blades, are investigated. The tapering effect in these laminated composite structures is introduced by terminating plies, which act as potential delamination sites. Delamination and uncertainties in material properties at various scales influence their dynamic behavior. The Variational Asymptotic Method (VAM) is used as a mathematical framework to develop a model of a tapered composite beam with delamination. Subsequently, the modal characteristics are obtained by coupling the VAM model with the reduced 1D FE beam model. Stochastic natural frequencies are investigated by combining the source uncertainties in the delaminated structure. Following a detailed validation study, the model capability is demonstrated on flexbeams typically used in helicopter rotor blades.

Keywords: Flexbeams, VAM, delamination, source uncertainties, stochastic modal analysis.

[*]Doctoral student, Department of Aerospace Engineering, Indian Institute of Technology, Bombay, Mumbai, India.
[**]Assistant professor, Department of Mechanical Engineering, K.J. Somaiya School of Engineering, Somaiya Vidyavihar University, Mumbai, Maharashtra, India.
[‡]PhD supervisor, Faculty, School of Engineering, Burgess Road, Southampton, UK, Email: S.Naskar@soton.ac.uk
[¶, §]Department of Aerospace Engineering, Indian Institute of Science, Banglore, Karnataka,560012, India.
[†]PhD supervisor, Department of Aerospace Engineering, Indian Institute of Technology, Bombay, Mumbai, India, Email : pjguru@aero.iitb.ac.in

1. Introduction

Tapered composite structures find applications in helicopter blades, yokes, turbine blades, etc. These structures have variable stiffness that is exploited to meet the design requirements. The best example of such a requirement in aerospace applications is a flexbeam structure utilized in helicopter rotor-blade assembly. These flexbeams require higher stiffness at the hub end, and flexibility at the blade end to accommodate the flapping motions [1].

Manufacturing of thickness-tapered composite beams is achieved by terminating or dropping the plies at pre-determined locations along the beam span [2]. The tapering effect in the beams reduces the stiffness due to the structural discontinuities formed because of ply dropping. In practice, the ply-dropping operation to terminate the plies generates resin pockets at the ply-drop locations, which are potential delamination nucleation sites. The combined influence of structural discontinuities in the tapered composite beams due to dropped-out plies and delamination strongly affects their static and dynamic performance. Hence, it is important to analyze their dynamic behavior since they are highly susceptible to vibrations [3]. This paper aims to focus on the free vibration analysis of tapered composite beams in healthy as well as delaminated conditions.

The review of literature on the free vibration response of tapered composite beams shows scarcity in experimental work and very few researchers have attempted this problem using analytical or numerical approaches [4]–[8]. One of the initial analytical works on modal analysis of a tapered composite beam is presented by Rao and Ganesan [9]. They proposed a Higher-order Shear Deformation Theory (HSDT) based finite element (FE) model. To simplify the model, they neglected the interlaminar shear deformation. Subequently, in their follow-up work, First-order Shear Deformation (FSDT) theory-based FE model [10] was used. The incorporation of shear deformations reduces the overestimated natural frequencies as obtained in the earlier model. FE-

based modeling of tapered composite beams was used by Gupta and Rao [11] to investigate the dynamic behavior of doubly tapered beams. Their study investigated the effect of beam width and thickness tapering. They noticed the strong influence of thickness tapering leading to the degradation of the cross-sectional stiffness and reduction in the beam's natural frequencies. In one more FE-based approach, the linearly tapered composite beam is modeled by a number of stepped Timoshenko beams, as presented by Tong *et al.*[12]. They validated their analytical model by comparing the free and forced vibration responses of beams with results available in the literature. In the development of numerical models of tapered composite beams, Zabihollah [13] implemented an advanced FE model based on which authors have presented the parametric results of natural frequencies for highlighting the influence of taper angle, boundary condition, and lay-up of the stack. Lin [14] has presented the implementation of hierarchical finite element formulation, which can use fewer elements, resulting in computational efficiency.

Few authors have reported advanced HSDT-based FE models indicating the vibration response of tapered laminated composite beams [13], [15], [16]. In these reported works, the tapered beams are modeled by considering three zones along the length of the beam: thick zone, thin zone, and tapered zone. Among these, the tapered zone contains the dropped-out plies, which are modeled as matrix-rich layers. One such work, based on HSDT formulation, is presented by Ganesan and co-authors [17] for analyzing the free vibration response of the tapered composite beams. In their extended work presented in [18], the effect of various parameters like taper angle, ply configurations, and boundary conditions are analyzed on the fundamental frequencies of thickness tapered composite beams. Also, the influence of various ply-dropping patterns on fundamental natural frequencies is presented in [18], suggesting an optimum choice of ply-dropping sequence to get comparatively lesser reductions in natural frequencies. In the experimental investigation of

tapered composite beams, one of the rarest studies on free vibration analysis is reported by Arumugam *et al.*[19] for a rotating beam. In this work, authors have also obtained the natural frequency results using HSDT-based analytical formulation which shows good agreement with the experimental investigation. The literature on free vibration analysis of delaminated tapered composite beams is very rare compared to that of delaminated uniform beams [20],[21]. One of the attempts to analyze the influence of delamination is addressed by Ghaffari *et al.* [22] and authors have presented the modal response of the thickness tapered composite beam for both healthy and delaminated conditions. Recently, Moorthy [23] has developed a surrogate-assisted algorithm that is designed based on the vibration response of a tapered composite beam to identify delamination severity. The reported literature on delaminated composite tapered beams highlights the influence of damage severity on the degradation of natural frequencies. This literature also highlights the complexities in modeling the delaminated configuration of tapered composite beams by using reported analytical frameworks or numerical models.

Due to the complexity of the manufacturing processes of laminated composites, there are uncertainties in the elastic properties and mass densities of fiber and matrix [24]–[29], which in turn affects the dynamic performance of the composite beams [30]–[34]. The propagation of these uncertainties at the macro level and further into the component level strongly affects the reliability of the structures due to stochastic response bounds of natural frequencies [35]–[38],[39]. Very few authors have addressed the issue of uncertainty analysis in the case of tapered composite beams. Kamali *et al.*[40] have employed a reliability-based design optimization method for free vibration analysis of tapered composite beams. Stochastic free vibration analysis of tapered composite beams under the influence of random variation in elastic modulus and mass densities is presented by Thi *et al.*[41]. The shortcoming of these available models is that multiple uncertain variables

are not being considered at a time in a single simulation. Experimental investigations for addressing uncertainties will demand large no. of samples to be tested, and it will not be possible to consider simultaneous uncertainties in all the micro or macro-properties of the composites in a single experiment [42]. Hence, the development of a stochastic computational platform for analyzing the random variations in natural frequencies of the composite tapered beams is required. This is the primary motivation of the proposed paper.

In this work, a computationally efficient VAM-based approach is proposed to simplify the problem into a 2D cross-sectional analysis and a 1D problem, similar to the framework presented in [43]. However, here the cross-sectional stiffness is determined at the uniform as well as the tapered sections in the presence of delamination. A simple 1D FE formulation is presented to showcase the model capability, similar to the work presented in [44],[45], but for a generic tapered composite structure. This coupled framework of VAM-1D FEM is easily extended to take the stochastic effects in uncertain material properties, and the respective stochastic distributions of natural frequencies are obtained. To the best of the author's knowledge, a VAM-based approach to model delaminated tapered composite beam and their stochastic dynamic behavior due to uncertain micro or macro-mechanical properties has not been addressed in the literature.

The structure of this paper hereafter is organized as follows: the proposed generalized five-layer cross-sectional stiffness model of the composite tapered beam is presented in section 2. The governing equations of motion are derived in section 3. The deterministic and stochastic frequency results are elaborately discussed and presented in section 4, and finally, the summarizing concluding remarks are included in section 5. The VAM-based cross-sectional stiffness terms derived for thick/thin and tapered zone sections of a tapered composite beam are elaborately given in the Appendix.

2. Generalized five-layer cross-sectional model of a tapered composite beam

In the case of tapered composite beams, the dropped-out plies are modeled by matrix-rich layers. Hence, these beams exhibit non-homogeneity across the cross-section due to the presence of matrix-rich plies along with normal plies. Due to this non-homogeneity, the estimation of the cross-sectional stiffness matrix is not a straightforward task for the cross-sections carrying dropped-out plies. To tackle this issue, a generalized five-layer cross-section model is proposed in this work for the non-homogeneous cross-section of a tapered composite beam carrying matrix-rich layers. This section particularly highlights how this proposed five-layer cross-section model works.

The typical geometry of a tapered composite beam with internal ply drops across the beam span is shown in Fig. 1(a). It shows the geometry schematic with three zones of the beam along the span; thick, tapered, and thin. The schematic of a generalized five-layer cross-section model proposed in this work for the non-homogeneous tapered zone section carrying dropped-out plies is presented in Fig. 1(b).

To implement the proposed five-layer model using the VAM framework, it is required to know the thicknesses of normal plies, dropped-out plies, and their corresponding positions measured from the mid-plane of a cross-section. In the symmetric ply drop model, as indicated in Fig. 1(b), few notations are used. The notation 'd_1' represents the total thickness of normal plies present above the mid-plane, and 'd_2' denotes the same below the mid-plane. The notation 'h' indicates the total thickness of normal plies present between two dropped-out plies that are adjacent to the mid-plane on the top and bottom sides of it. The total thicknesses of dropped-out plies above and below the mid-plane are indicated by notations't_1' and 't_2' respectively. This generalized five-layer

cross-section model of the tapered composite beam can be applied to any ply drop configuration. The various configurations of ply dropping like external ply drop-off, middle ply drop-off, or internal ply drop-off are mentioned in a detailed review article on tapered composite beams in [21].

In the case of symmetric-external ply drop-off, the model will be generalized with three layers due to the dropping of outer plies adjacent to the top and bottom surfaces of the cross-section. Similarly, in the case of internal ply drop-off with middle plies dropped configuration, '*h*' value will be zero which makes the model generalized with four layers. In this way, this proposed model can be applied to delaminated sublaminates in the case of delaminated tapered composite beams.

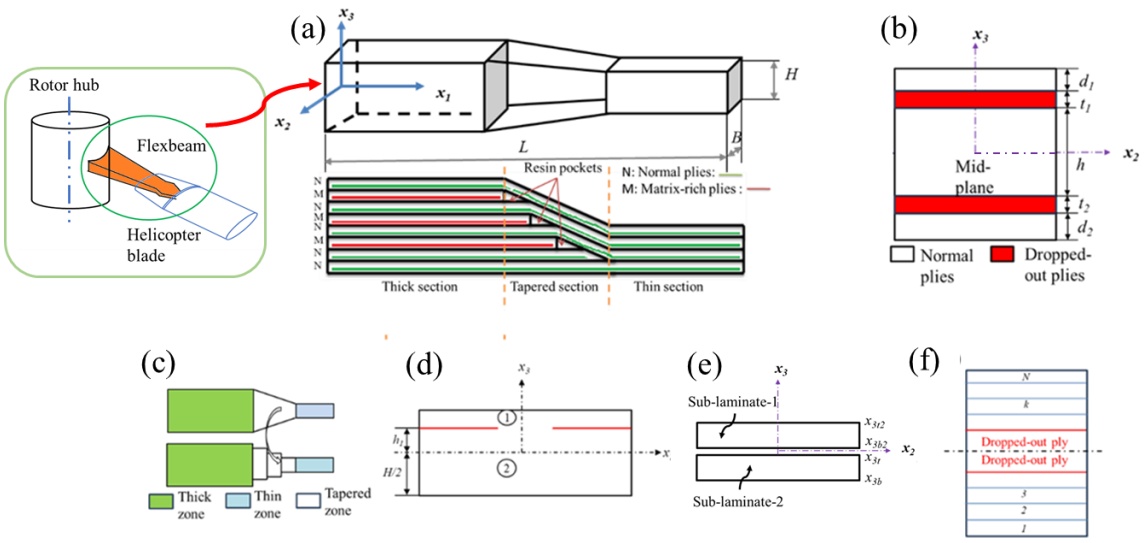

Fig. 1 Tapered composite beam geometry and modeling details: (a) Tapered beam geometry schematic showing different zones, (b) Proposed generalized five-layer cross-section model of taper zone, (c) Proposed FE model approach, (d) Beam cross-section representing delamination location, (e) schematic of the sublaminates formation due to Full-width delamination across the thickness of a cross-section, (f) Generalized ply lay-up sequence in the tapered zone of a beam showing layer numbers

3. Governing equations of free vibration analysis of tapered composite beams

In this section, the governing equations of the natural frequencies of free vibration of a thickness-tapered composite beam are derived. The geometrical schematic of the composite tapered beam is

shown in Fig. 1(a). The coordinate system (x_1,x_2,x_3) is considered where the length (L), width (B), and thickness (H) of a beam are taken along x_1, x_2, and x_3 coordinates, respectively, as shown in Fig. 1(a). The limits of coordinates are as: $0 \le x_1 \le L$, $-B/2 \le x_2 \le B/2$, $-H/2 \le x_3 \le H/2$.

The proposed approach implements a coupled framework of VAM and 1D FEM for the estimation of the cross-sectional stiffness matrix and natural frequencies of composite tapered beams. For the convenience of FE-based modeling, the span of the thickness-tapered composite beam is divided into three zones: thick, tapered, and thin zones, as indicated in Fig. 1(a). As the tapered zone is non-homogeneous due to dropped-out plies, its cross-sectional stiffness estimation is more complex as compared to that of homogeneous thick/thin zones. Hence, this section presents the separate derivations for 1D cross-sectional stiffness terms of tapered as well as non-tapered zones of healthy and delaminated beams by using a VAM framework. For the derivation of cross-sectional stiffness matrices using the VAM framework for thick, tapered, and thin zones of a tapered beam, each zone is considered as prismatic beam. Out of the three zones, thick and thin zones are homogeneous prismatic beam sections, whereas the tapered zone is a non-homogeneous prismatic beam section due to the presence of terminated plies which are modeled as matrix-rich layers. According to the no. of plies terminated in the tapered beam, the tapered zone is approximated by modeling it as a stepped section with multiple prismatic non-homogeneous cross-sections, as shown in Fig. 1(c). The cross-sectional stiffness matrix terms of each zone are derived individually in the form of closed-form expressions, as elaborately discussed in subsequent discussions.

Following the VAM approach, detailed in [46], [47] the strain energy formulation for the tapered composite beam is done by using the geometrical small parameter of its thickness-to-length ratio (δ_h) and material small parameters of maximum allowable strains (ε). To obtain the 3D strain

energy density expression for a single layer of any zone of a tapered composite beam, a tapered zone with a generalized ply lay-up of N laminae is considered, as shown in Fig. 1(f). For an arbitrary k^{th} layer from a stack of generalized tapered zones of a beam, the 3D strain energy density (U_{3D}^{K}) is given in eq. (1).

$$U_{3D}{}^{k} = \begin{Bmatrix} \Gamma_{11}{}^{k} \\ \Gamma_{22}{}^{k} \\ \Gamma_{33}{}^{k} \\ 2\Gamma_{23}{}^{k} \\ 2\Gamma_{13}{}^{k} \\ 2\Gamma_{12}{}^{k} \end{Bmatrix}^{T} \begin{bmatrix} C_{11}{}^{k} & C_{12}{}^{k} & C_{13}{}^{k} & 0 & 0 & 0 \\ C_{12}{}^{k} & C_{22}{}^{k} & C_{23}{}^{k} & 0 & 0 & 0 \\ C_{13}{}^{k} & C_{32}{}^{k} & C_{33}{}^{k} & 0 & 0 & 0 \\ 0 & 0 & 0 & C_{44}{}^{k} & 0 & 0 \\ 0 & 0 & 0 & 0 & C_{55}{}^{k} & 0 \\ 0 & 0 & 0 & 0 & 0 & C_{66}{}^{k} \end{bmatrix} \begin{Bmatrix} \Gamma_{11}{}^{k} \\ \Gamma_{22}{}^{k} \\ \Gamma_{33}{}^{k} \\ 2\Gamma_{23}{}^{k} \\ 2\Gamma_{13}{}^{k} \\ 2\Gamma_{12}{}^{k} \end{Bmatrix} \tag{1}$$

where, Γ_{ij}^{k} represents the 3D strains of a considered k^{th} lamina, and C_{ij}^{k} represents the material stiffness matrix terms of k^{th} lamina. The same expression of 3D strain energy density of a dropped-out lamina, which is modeled as a matrix-rich layer, can be written similarly to eq. (1) but by just replacing the ply material stiffness matrix (C_{ij}^{k}) with resin material stiffness matrix terms ($C_{r_{ij}}{}^{k}$). In the case of a lamina with an arbitrary ply angle (θ), the material stiffness matrix (C_{ij}^{k}) of a lamina should be transformed from its material coordinate system to the global coordinate system of a beam. The transformed material stiffness matrix ($\overline{C_{ij}^{k}}$) for k^{th} lamina with an arbitrary ply angle (θ) is given by eq. (2),

$$\overline{C}_{ij}{}^{k} = \{T\}^{T} \left[C_{ij}{}^{k} \right] \{T\} \tag{2}$$

where, T is the transformation matrix for the lamina, and the respective matrix terms of it are functions of ply angle θ. The total 3D strain energy density of the considered tapered zone of a beam, as indicated in Fig. 1(f), is given in eq. (3). It is a sum of 3D strain energy densities of

normal plies and that of terminated plies (which are modeled as matrix-rich layers) present in the stack

$$U_{3D} = \sum_{k=1}^{N-4} \left\{\Gamma_{ij}^{\ k}\right\}^T \left[\overline{C_{ij}^{k}}\right] \left\{\Gamma_{ij}^{\ k}\right\} + \sum_{k=N-4}^{N-2} \left\{\Gamma_{ij}^{\ k}\right\}^T \left[\overline{Cr_{ij}^{k}}\right] \left\{\Gamma_{ij}^{\ k}\right\} + \sum_{k=N-2}^{N} \left\{\Gamma_{ij}^{\ k}\right\}^T \left[\overline{C_{ij}^{k}}\right] \left\{\Gamma_{ij}^{\ k}\right\} \quad (3)$$

$$Considering, \sum_{k=1}^{N} \left[\overline{C}_{ij}^{\ k}\right] = \left[C_{ij}\right]$$

$$U_{3D} = \left\{\Gamma_{ij}^{\ k}\right\}^T \left[C_{ij}\right] \left\{\Gamma_{ij}^{\ k}\right\}$$

where, U_{3D} denotes the total 3D strain energy density of the considered tapered zone. By following the similar procedure given in eq. (1) - eq. (3) for the tapered zone, the 3D strain energy densities for thick and thin zones of a beam containing only normal plies, can also be calculated. The total 3D strain energy density (U_{3D}) for a particular zone of a beam is given by eq. (4).

$$U_{3D} = \frac{1}{2} \begin{pmatrix} \Gamma_{11} \\ \Gamma_{22} \\ \Gamma_{33} \\ 2\Gamma_{23} \\ 2\Gamma_{13} \\ 2\Gamma_{12} \end{pmatrix}^T \begin{bmatrix} C_{11} & C_{12} & C_{13} & 0 & 0 & 0 \\ C_{12} & C_{22} & C_{23} & 0 & 0 & 0 \\ C_{13} & C_{23} & C_{33} & 0 & 0 & 0 \\ 0 & 0 & 0 & C_{44} & 0 & 0 \\ 0 & 0 & 0 & 0 & C_{55} & 0 \\ 0 & 0 & 0 & 0 & 0 & C_{66} \end{bmatrix} \begin{pmatrix} \Gamma_{11} \\ \Gamma_{22} \\ \Gamma_{33} \\ 2\Gamma_{23} \\ 2\Gamma_{13} \\ 2\Gamma_{12} \end{pmatrix} \quad (4)$$

where C_{ij} represents transformed 3D material stiffness matrix terms for the thick/thin/tapered zone of a beam in global coordinates, and Γ_{ij} terms represent respective 3D strains.

The generalized expressions of 3D strain measures (Γ_{ij}) of a tapered beam zone which are expressed in terms of 1D strains (Υ_{ij}), 1D curvatures (K_i), and cross-sectional warpings (w_i) are explicitly presented in [46] and given in eq. (5). These expressions of 3D strains are obtained by considering the position vectors of any material point on a reference curve of the beam in its deformed and undeformed states. In the undeformed state, the position vector of a point on the reference curve of a beam is represented in the form of longitudinal and transverse shear strains.

However, in the deformed state, the position vectors are expressed in the form of bending and twisting curvatures as well as cross-sectional warpings. The deformation gradient tensor relates the position of a material point on the reference curve of a beam in the initial undeformed configuration with its respective position in the deformed configuration. It is obtained by considering the covariant and contravariant bases of deformed and undeformed states of a beam. Based on the terms of deformation gradient tensor, the 3D strains are obtained as given in eq. (5) for a particular zone of a tapered beam. The detailed equations and illustrations on these 3D strain expressions can be referred to from [46].

$$
\begin{aligned}
\Gamma_{11}^{(1,2)} &\approx \gamma_{11} + \left(x_3 \pm \bar{h}\right) K_2 - x_2 K_3 + \underline{\frac{\partial w_1^{(1,2)}}{\partial x_1} - K_3 w_2^{(1,2)} + K_2 w_3^{(1,2)}} \\
\Gamma_{22}^{(1,2)} &\approx \frac{\partial w_2^{(1,2)}}{\partial x_2} \\
\Gamma_{33}^{(1,2)} &\approx \frac{\partial w_3^{(1,2)}}{\partial x_3} \\
2\Gamma_{23}^{(1,2)} &\approx \frac{\partial w_2^{(1,2)}}{\partial x_3} + \frac{\partial w_3^{(1,2)}}{\partial x_2} \\
2\Gamma_{13}^{(1,2)} &\approx 2\gamma_{13} + \frac{\partial w_1^{(1,2)}}{\partial x_3} + x_2 K_1 + \underline{w_2^{(1,2)} K_1 - w_1^{(1,2)} K_2 + \frac{\partial w_3^{(1,2)}}{\partial x_1}} \\
2\Gamma_{12}^{(1,2)} &\approx 2\gamma_{12} + \frac{\partial w_1^{(1,2)}}{\partial x_2} - \underline{\left(x_3 \pm \bar{h}\right) K_1 - w_3^{(1,2)} K_1 - w_1^{(1,2)} K_3 + \frac{\partial w_2^{(1,2)}}{\partial x_1}}
\end{aligned}
\tag{5}
$$

where $\Gamma_{11}, \Gamma_{22}, \Gamma_{33}$ are longitudinal 3D strains, Υ_{ij} represent 1D strains (longitudinal and shear components), K_1, K_2, and K_3 denote 1D curvatures (bending and twisting), and w_1, w_2, and w_3 are cross-sectional warpings of a particular zone of composite tapered beam. In eq. (5), the underlined terms indicate non-linear terms arise due to moderate local rotations. The term $\bar{h}$ in the eq. (5) appears only in the case of delaminated beams as it represents the delamination location introduced across the thickness of a beam by shifting the x_3 coordinate along the thickness direction according

to the sublaminate approach which is detailed in [43], [44], [48]. The superscripts *1* and *2* in the eq. (5) respectively indicate the sublaminate numbers 1 and 2 for a single delamination case forming two sublaminates as shown in Fig. 1(d) and 1(e). The expression of the term $\bar{h}$ in eq. (5) for sublaminate 1 as shown in Fig. 1(d) is given by eq. (6).

$$\bar{h} = \frac{\frac{H}{2} - h_1}{2} \tag{6}$$

where h_1 denotes the delamination location across the thickness of a beam measured from the mid-plane (refer to Fig. 1(d)).

Before implementing the VAM framework, the order analysis is required to be carried out which helps to decide the appropriate terms that are to be considered in the formulation of strain energy. In this paper, zeroth order analysis is carried out which suggests the retention of only zeroth order strain energy terms from the strain energy expression. According to this, from eq. (5), only the non-underlined terms are considered in the further formulation. In zeroth order analysis, the order of warping is εH, where ε denotes the small strain parameter and H is the small characteristic dimension of the cross-section (thickness of the beam cross-section). The longitudinal strains ($\gamma_{11}, \gamma_{22}, \gamma_{33}$) are of order ε, transverse shear strains ($\gamma_{12}, \gamma_{23}, \gamma_{13}$) are of order $\varepsilon\delta_h$ and the curvatures (K_1, K_2, K_3) are of order ε/H. By following this zeroth order analysis, the reduced expressions of 3D strains in the form of 1D strains, 1D curvatures, and cross-sectional warping are expressed in eq. (7).

$$
\begin{aligned}
\Gamma_{11}^{(1,2)} &\approx \gamma_{11} + \left(x_3 \pm \bar{h}\right) K_2 - x_2 K_3 \\
\Gamma_{22}^{(1,2)} &\approx \frac{\partial w_2^{(1,2)}}{\partial x_2} \\
\Gamma_{33}^{(1,2)} &\approx \frac{\partial w_3^{(1,2)}}{\partial x_3} \\
2\Gamma_{23}^{(1,2)} &\approx \frac{\partial w_2^{(1,2)}}{\partial x_3} + \frac{\partial w_3^{(1,2)}}{\partial x_2} \\
2\Gamma_{13}^{(1,2)} &\approx 2\gamma_{13} + \frac{\partial w_1^{(1,2)}}{\partial x_3} \\
2\Gamma_{12}^{(1,2)} &\approx 2\gamma_{12} + \frac{\partial w_1^{(1,2)}}{\partial x_2}
\end{aligned}
\tag{7}
$$

By substituting eq. (7) into eq. (4), an expression for the 3D strain energy density of a particular zone of a tapered composite beam is obtained in the form of 1D strains (Υ_{ij}), 1D curvatures (K_i), and cross-sectional warpings (w_i). Because of six 1D generalized strain measures and three warping measures in the strain energy formulation, there are large no. of unknown variables in the model. To overcome this issue, a set of six constrained equations, collectively included in eq. (8) are imposed while solving for unknown warpings.

$$
\int_{-H/2}^{H/2} \int_{-B/2}^{B/2} w_i(x_{1,} x_{2,} x_{3,}) dx_2 dx_3 = 0 \ldots\ldots (i = 1,2,3)
\tag{8}
$$

$$
\int_{-H/2}^{H/2} \int_{-B/2}^{B/2} \left(\frac{\partial w_i(x_{1,} x_{2,} x_{3,})}{\partial x_j} - \frac{\partial w_j(x_{1,} x_{2,} x_{3,})}{\partial x_i} \right) dx_2 dx_3 = 0 \ldots\ldots (i \neq j)
$$

where, w_2 and w_3 are in-plane warpings and w_1 represents out-of-plane warping for a cross-section of a beam. The expression of 1D strain energy density (U_{1D}) which is directly derived from 3D strain energy density (U_{3D}) is given in eq. (9).

$$U_{1D} = \int_{-H/2}^{H/2} \int_{-B/2}^{B/2} U_{3D} dx_2 dx_3 \tag{9}$$

For a particular zone of a tapered composite beam problem, 1D strain energy density (U_{1D}) is expressed in the form of 1D strain measures as given in eq. (10).

$$U_{1D} = \int_{-H/2}^{H/2} \int_{-B/2}^{B/2} \begin{Bmatrix} \gamma_{11} \\ \gamma_{22} \\ \gamma_{33} \\ 2\gamma_{23} \\ 2\gamma_{13} \\ 2\gamma_{12} \end{Bmatrix}^T \begin{bmatrix} C_{11} & C_{12} & C_{13} & 0 & 0 & 0 \\ C_{21} & C_{22} & C_{23} & 0 & 0 & 0 \\ C_{31} & C_{32} & C_{33} & 0 & 0 & 0 \\ 0 & 0 & 0 & C_{44} & 0 & 0 \\ 0 & 0 & 0 & 0 & C_{55} & 0 \\ 0 & 0 & 0 & 0 & 0 & C_{66} \end{bmatrix} \begin{Bmatrix} \gamma_{11} \\ \gamma_{22} \\ \gamma_{33} \\ 2\gamma_{23} \\ 2\gamma_{13} \\ 2\gamma_{12} \end{Bmatrix} dx_2 dx_3 \tag{10}$$

The closed-form expressions for the cross-sectional stiffness terms (S_{ij}) of thick, tapered, and thin zones of the tapered composite beam are extracted from the 1D strain energy density (U_{1D}) expression given in eq. (10) by using eq. (11).

$$S_{ij} = \frac{\delta U_{1D}}{\delta \gamma_i \delta \gamma_j} \tag{11}$$

Here, S_{ij} is a *6 X 6* cross-sectional stiffness matrix of a particular zone of a tapered beam. The detailed formulation of elements of this matrix for tapered (with matrix-rich plies) and thick/thin (without matrix-rich plies) zones of a tapered composite beam are elaborately derived and presented in the next sub-section and Appendix.

3.1 Formulation of the stiffness matrix of the non-tapered zone

At first, the cross-section of the non-tapered zone without matrix-rich plies indicated by thick and thin zone sections of a tapered composite beam is considered for the analysis. The 3D strain energy density expression for a thick/thin zone of a beam is obtained as given in eq. (4). As per the VAM

procedure [43], the variational form of 3D strain energy gives a set of governing equations in the form of second-order partial differential equations (PDEs) and associated boundary conditions. These coupled partial differential equations are presented in eq. (12) in which w_1, , w_2 and w_3 are the unknown warpings.

$$
\begin{aligned}
&-C_{55}\frac{\partial^2 w_1}{\partial x_3{}^2}-C_{66}\frac{\partial^2 w_1}{\partial x_2{}^2}=0\\
&C_{12}K_3-C_{44}\frac{\partial^2 w_2}{\partial x_3{}^2}-\left(C_{23}+C_{44}\right)\frac{\partial w_3}{\partial x_2\partial x_3}-C_{22}\frac{\partial^2 w_2}{\partial x_2{}^2}=0\\
&-C_{13}K_2-C_{33}\frac{\partial^2 w_3}{\partial x_3{}^2}-\left(C_{23}+C_{44}\right)\frac{\partial w_2}{\partial x_2\partial x_3}-C_{44}\frac{\partial^2 w_3}{\partial x_2{}^2}=0
\end{aligned}
\tag{12}
$$

As it is difficult to solve the coupled PDEs given in eq. (12) for unknown warpings, the solution polynomials are assumed for these in-plane (w_2 and w_3) and out-of-plane (w_1) warpings separately. Here, for in-plane warpings power series solution polynomials in terms of material stiffness matrix terms (C_{ij}) and cross-sectional coordinates x_2 and x_3 are assumed. The out-of-plane warping is obtained by assuming a trigonometric solution polynomial. These assumed warping solutions for non-tapered (thick and thin zones) cross-sections are mentioned in the Appendix (refer to eq. (A_5)). The accuracy of the choice of the warping solutions is verified by checking if they satisfy the PDEs obtained earlier.

After substituting the assumed warping solutions in 3D strain energy density expression, the reduced 1D strain energy density (U_{1D}) is obtained as discussed in eq, (9), and eq. (10). Corresponding to the assumed zeroth order warping solutions, the zeroth order cross-sectional stiffness matrix is derived by taking the second derivative of the 1D strain energy density concerning corresponding 1D strain energy measures. The stiffness matrix terms represented by S_{ij}^{nH} in eq. (13) are elaborately given in Appendix (refer to eq. (A_1)) for a non-tapered zone cross-

section. Here, the superscript *nH* is used to denote the stiffness terms of a healthy non-tapered cross-section (healthy thick/thin sections of a tapered composite beam). The off-diagonal stiffness terms of matrix S_{ij}^{nH} are derived to be zero as the proposed formulation is derived for thick and thin zone sections of symmetric lay-up.

$$U_{1D} = \begin{Bmatrix} \gamma_{11} \\ 2\gamma_{12} \\ 2\gamma_{13} \\ k_1 \\ k_2 \\ k_3 \end{Bmatrix}^T \begin{bmatrix} S_{11}^{nH} & 0 & 0 & 0 & 0 & 0 \\ 0 & S_{22}^{nH} & 0 & 0 & 0 & 0 \\ 0 & 0 & S_{33}^{nH} & 0 & 0 & 0 \\ 0 & 0 & 0 & S_{44}^{nH} & 0 & 0 \\ 0 & 0 & 0 & 0 & S_{55}^{nH} & 0 \\ 0 & 0 & 0 & 0 & 0 & S_{66}^{nH} \end{bmatrix} \begin{Bmatrix} \gamma_{11} \\ 2\gamma_{12} \\ 2\gamma_{13} \\ k_1 \\ k_2 \\ k_3 \end{Bmatrix} \tag{13}$$

3.2 Formulation of the stiffness matrix of the tapered zone

In this sub-section, the stiffness matrix for the tapered zone of a beam, which contains normal layers along with the dropped-out plies, which are modeled as matrix-rich layers, is derived using VAM. Due to the non-homogeneity of the tapered zone, different warping solutions for different layers (matrix-rich or non-matrix-rich) are assumed. To make the model simpler, a set of generalized warping solutions individually for matrix-rich and non-matrix-rich layers is assumed in this proposed work. These assumed generalized solutions for three warpings are presented in Appendix (refer Appendix eq. A_6). To accurately assume these warping solutions for a particular layer or group of layers, a generalized five-layer cross-section model is implemented, which is shown in Fig. 1(b) and discussed elaborately in section 2.

The procedure of obtaining coupled PDEs and boundary conditions by implementing variational formulation is the same as that mentioned for the non-tapered zone in the earlier sub-section. The stiffness terms S_{ij}^{mH} presented in eq. (14) are obtained by taking the second derivative of the 1D strain energy density of a tapered zone of a beam concerning corresponding 1D strain measures as

given in eq. (11). The derived stiffness matrix terms (S_{ij}^{mH}) are elaborately expressed in eq. (A_2) of Appendix for the tapered zone of a beam. Here superscript *mH* stands for healthy cross-section with matrix-rich plies (tapered zone). It is observed that along with diagonal stiffness terms, off-diagonal stiffness terms like S_{15}^{mH} and S_{24}^{mH} appear in the stiffness matrix of the tapered zone. This is due to the presence of structural couplings for a particular lay-up of a tapered zone of the beam. Also, these terms arise due to non-homogeneity and asymmetry of the tapered zone due to terminated plies.

$$U_{1D} = \begin{Bmatrix} \gamma_{11} \\ 2\gamma_{12} \\ 2\gamma_{13} \\ k_1 \\ k_2 \\ k_3 \end{Bmatrix}^T \begin{bmatrix} S_{11}^{mH} & 0 & 0 & 0 & S_{15}^{mH} & 0 \\ 0 & S_{22}^{mH} & 0 & S_{24}^{mH} & 0 & 0 \\ 0 & 0 & S_{33}^{mH} & 0 & 0 & 0 \\ 0 & S_{24}^{mH} & 0 & S_{44}^{mH} & 0 & 0 \\ S_{15}^{mH} & 0 & 0 & 0 & S_{55}^{mH} & 0 \\ 0 & 0 & 0 & 0 & 0 & S_{66}^{mH} \end{bmatrix} \begin{Bmatrix} \gamma_{11} \\ 2\gamma_{12} \\ 2\gamma_{13} \\ k_1 \\ k_2 \\ k_3 \end{Bmatrix} \tag{14}$$

3.3 Stiffness matrix of a delaminated tapered beam

After the determination of healthy cross-sectional stiffness matrix terms of a composite tapered beam, the damaged stiffness matrix terms of delaminated tapered beams are derived in this sub-section. The estimation of cross-sectional stiffness terms of delaminated beams is done by following the sublaminate approach as mentioned in [44]. Two separate sublaminates formed due to full-width delamination are shown in Fig. 1(f). The 1D strain energy density for two sub-laminates is given by eq. (15-a) and eq. (15-b).

$$U_{1D}^{(1)} = \int_{x_{3b}}^{x_{3t}} \int_{-B/2}^{B/2} U_{3D} dx_2 dx_3 \tag{15-a}$$

$$U_{1D}^{(2)} = \int_{x_{3b2}}^{x_{3t2}} \int_{-B/2}^{B/2} U_{3D} dx_2 dx_3 \tag{15-b}$$

where superscripts *(1)* and *(2)* indicate the respective strain energy densities for sublimates 1 and 2, respectively. The terms x_{3b} and x_{3t} denote the positions of the bottommost layer and the topmost layer for the first sublaminate, while the notations x_{3b2} and x_{3t2} indicate the respective terms for sub-laminate 2. The proposed customized five-layer cross-section model is utilized for determining cross-sectional stiffnesses of delaminated sublaminates by using the VAM framework. Eq. (16) is used to obtain the cross-sectional stiffness terms from 1D strain energy expression for individual sub-laminates, which are clubbed together to obtain cross-sectional stiffness matrix terms of the delaminated tapered composite beam.

$$S_{ij}^{(1)} = \frac{\delta U_{1D}^{(1)}}{\delta \gamma_i \delta \gamma_j}, S_{ij}^{(2)} = \frac{\delta U_{1D}^{(2)}}{\delta \gamma_i \delta \gamma_j} \tag{16}$$

For the case of partial width delamination, the strain energy density expression is to be written for small sub-intervals across the width due to delamination. The strain energy density for the delaminated (partial width) beam is given by eq. (17) in which superscripts (1) and (2) denote sub-laminate numbers, x_{2l} and x_{2r} indicate the locations of delamination from the origin towards the left and right sides across the width.

$$\begin{aligned} U_{1D} = &\int_{-H/2}^{H/2} \int_{-B/2}^{-x_{2l}} U_{3D}^{(1)} dx_2 dx_3 + \int_{-H/2}^{H/2} \int_{-x_{2l}}^{-x_{2r}} U_{3D}^{(1)} dx_2 dx_3 + \int_{-H/2}^{H/2} \int_{x_{2r}}^{B/2} U_{3D}^{(1)} dx_2 dx_3 + \ldots \\ &\int_{-H/2}^{H/2} \int_{-x_{2l}}^{-x_{2r}} U_{3D}^{(2)} dx_2 dx_3 + \int_{-H/2}^{H/2} \int_{-x_{2l}}^{x_{2r}} U_{3D}^{(1)} dx_2 dx_3 + \int_{-H/2}^{H/2} \int_{x_{2r}}^{B/2} U_{3D}^{(1)} dx_2 dx_3 \end{aligned} \tag{17}$$

The stiffness terms of delaminated sections are derived analytically by following the same approach as mentioned in the previous sections for determining the stiffness of healthy cross-sections. The delaminated cross-sectional stiffness terms (S^{mD}) are given in the Appendix in eq. (A_3), where superscript *mD* refers to the delaminated tapered section containing matrix-rich plies.

3.4 Eigenvalue problem formulation for natural frequencies of free vibration

For the reduced one-dimensional FE beam model, a generalized beam element with two nodes having six degrees of freedom per node is implemented. These six DOFs include three translations, two rotations, and one twist. The natural frequency of free vibration of the tapered composite beam is given by characteristic eq. (18) [44].

$$\left[[K]-[M]\omega^2\right]\{u\}=0 \tag{18}$$

where $[K]$ and $[M]$ are the global stiffness and mass matrices respectively of a tapered composite beam which are calculated by an assemblage of individual element stiffness matrices and individual mass matrices of thick, tapered, and thin zone sections. In eq. (18), $\{u\}$ denotes the nodal degree of freedom vector, and ω denotes the natural frequency vector of free vibration.

The present work also addresses the uncertainties in micro-mechanical properties, because of which the natural frequencies of a tapered composite beam are stochastic. In this work, to account for uncertainties in fiber and matrix properties of tapered composite beams at the micro-scale, random virtual samples of each property are generated using Monte Carlo Simulations. To denote the uncertainty of a particular parameter, a notation ($\bar{S}$) is used in association with the uncertain parameter. For example, the uncertain property matrix at micro-scale is indicated as $p(\bar{S})$ and is given in eq. (19).

$$p\left(\bar{S}\right)=\left\{E_{1f}\left(\bar{S}\right),E_{2f}\left(\bar{S}\right),G_f\left(\bar{S}\right),\nu_{12f}\left(\bar{S}\right),E_m\left(\bar{S}\right),G_m\left(\bar{S}\right),\nu_{12m}\left(\bar{S}\right),V_f\left(\bar{S}\right)\right\} \tag{19}$$

In eq. (19), all the micro-properties of fiber and matrix denoted by subscripts *f* and *m* respectively are uncertain, along with uncertainty in volume fraction (V_f) as well. Uncertainties at the micro-scale are propagated to the macro-scale and eventually, material stiffness matrix terms are stochastic which can be denoted by $C_{ij}(\bar{S})$. Due to uncertainties in the material stiffness matrix, the cross-sectional stiffness of the tapered composite beam is stochastic. The deterministic eigenvalue problem formulation for natural frequency expressed in characteristic eq. (18) is extended further to take uncertain inputs and the corresponding equation for stochastic frequencies is formulated as given in eq. (20).

$$\left[\left[K_s\right]-\left[M_s\right]\omega_s^2\right]\{u\}=0 \tag{20}$$

where $[K_s]$,$[M_s]$, ω_s represent stochastic global stiffness matrix, stochastic mass matrix, and stochastic natural frequency vector, respectively. Stochasticity in global stiffness matrix ($[K_s]$) is due to uncertainty in the cross-sectional stiffness matrix, as discussed earlier. The stochasticity in the mass matrix ($[M_s]$) is due to consideration of uncertainty in mass densities of fiber ($\rho_f(\bar{S})$) and matrix ($\rho_m(\bar{S})$) of a composite tapered beam. The graphical representation highlighting the stochastic analysis scheme proposed in this work in the form of a flow chart for analyzing the dynamic response of a tapered composite beam is presented in Fig. 2.

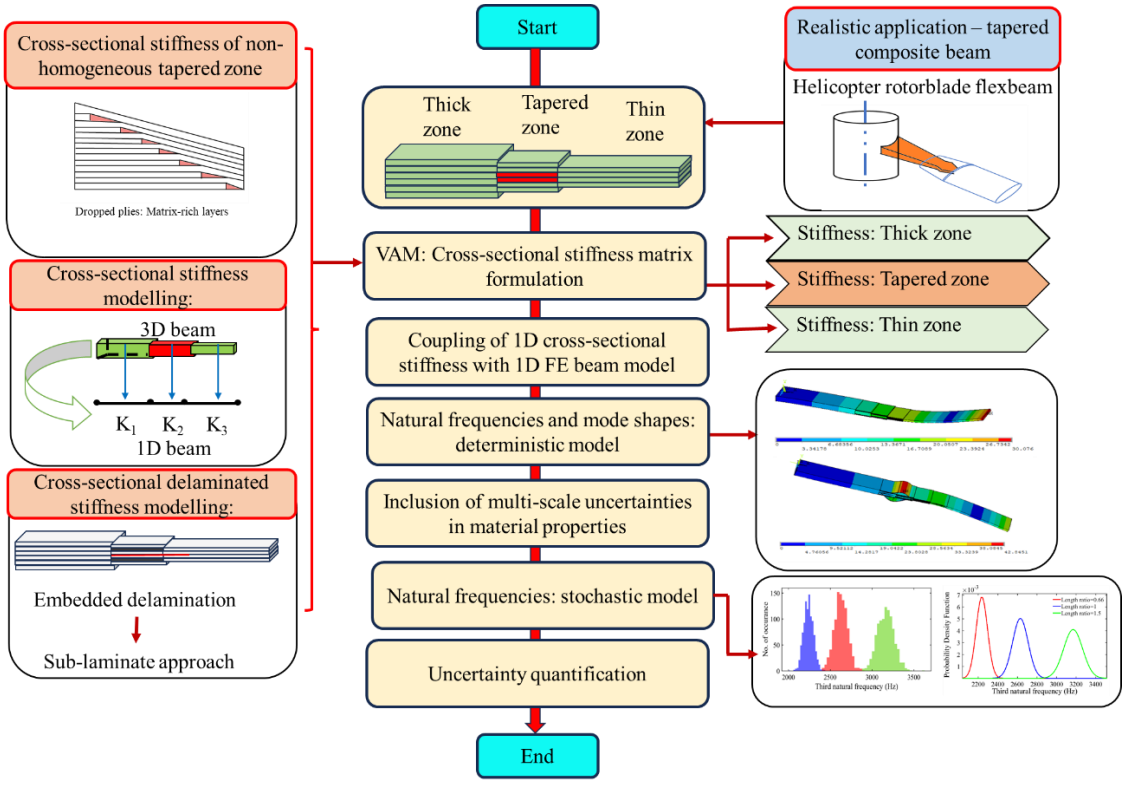

Fig. 2 Proposed stochastic dynamic analysis scheme for a tapered composite beam

4. Results and discussions

In this section, we present the free vibration response of composite tapered beams, which are modeled by dropping out the internal plies. This response is presented in the form of deterministic and stochastic results of natural frequencies. The implementation of a coupled computational framework based on a combination of VAM-based one-dimensional FE model is proposed here to estimate the natural frequencies of the healthy and delaminated tapered composite beams. First, the validation of the proposed model is carried out by comparing the natural frequencies of healthy and delaminated tapered composite beams with the results available in the literature [19], [22]. After the validation study, the proposed deterministic model is extended to the development of the stochastic dynamic analysis framework for the composite tapered beams.

4.1 Validation study

In this sub-section, the deterministic dynamic response of healthy and delaminated composite tapered beams measured in the form of natural frequencies is validated with the experimental and analytical results reported in the literature.

Table 1 Material and geometry details of tapered composite beams

Attribute	Arumugam *et al.*[19]	Ghaffari *et al.*[22]
Material details		
Longitudinal modulus (E_1)	31.38 GPa	113.9 GPa
Transverse modulus (E_2)	7.15 GPa	7.9856 GPa
Poisson's ratio	0.276	0.288
In-plane shear modulus (G_{12})	2.87 GPa	3.138 GPa
Mass density	1745 kg/m^3	1480 kg/m^3
Geometry details		
Lay-up of thick section	$[0/90]_{8s}$	$[0/90]_{9s}$
Lay-up of thin section	$[0/90]_{4s}$	$[0/90]_{3s}$
No. of dropped-out plies	16	24
Length of a beam (L)	300 mm	129 mm
Length of thick section	100 mm	50 mm
Length of thin section	100 mm	50 mm
Width (w)	50 mm	15 mm
Ply thickness (t_p)	0.19 mm	0.125 mm

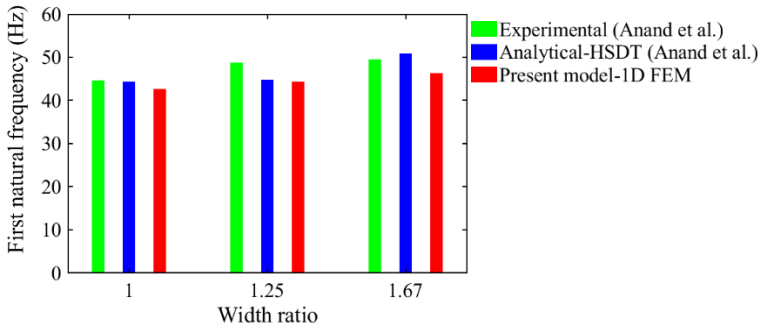

Fig. 3 Validation of tapered composite beams with experimental and 3D FEM results

4.1.1 Validation for healthy tapered composite beam model

In the deterministic analysis of a healthy composite tapered beam, at first, the validation study of a proposed model is carried out by comparing the fundamental natural frequency results with experimental investigations and analytical results presented by Arumugam *et al.* [15]. The details

of the geometry and material properties for the doubly tapered (tapering effect along width and thickness directions) glass-epoxy laminated composite beam are given in Table 1 (Arumugam *et al.*[19]). The fundamental natural frequency of free vibration under clamped-free boundary conditions and with three different width ratios are obtained by using the proposed model, and results are compared with reported results [19] as shown in Fig. 3.

The comparison shows very close agreement (within 10% deviations) of the fundamental natural frequencies obtained from the proposed model and published experimental as well as analytical results presented in [19]. The frequencies reported from the experimental work are relatively higher compared to the results from the proposed model. For three different width ratios mentioned in Fig. 3, the frequencies reported from the experimental work are 4.42%, 4.76%, and 6.49% higher as compared to fundamental frequency values from the proposed model. It is worthwhile to note from Fig. 3 that the percentage deviation in the fundamental natural frequencies obtained from the proposed model and reported analytical model, which also considers the transverse shear deformations, is within 5% for the range of width ratios investigated in the study.

After this validation, another geometry of a tapered composite beam analyzed by Ghaffari et al. [22] in their vibration-based damage detection work is considered for further results of deterministic natural frequencies. The effect of delamination on the natural frequencies of a tapered composite beam is investigated in this work. The geometry and material property details of this tapered composite beam are mentioned in Table 1 (Ghaffari et al. [22]). The ply drop configuration of 'D type' as suggested in [22] is considered for modeling a tapering section with 24 dropped-out plies. The natural frequency results are compared with published results in [22] which are based on higher-order FEM formulations and also with the 3D FE model of the tapered composite beam executed in this work. The deterministic dynamic analysis results highlighting the

first three bending natural frequencies of a cantilever tapered composite beam are shown in Fig. 4 (a). The natural frequencies obtained from the proposed model by considering and ignoring transverse shear deformations across the thickness of the beam are included in Fig. 4(a) for comparison.

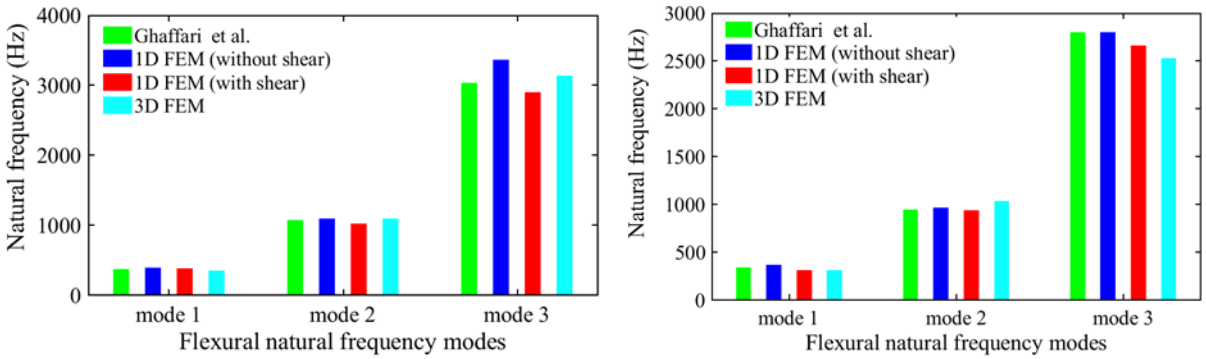

(a) (b)

Fig. 4 Validation of deterministic natural frequency results of (a) healthy tapered composite beam (b) delaminated tapered composite beam

The natural frequencies of the first three bending modes obtained from the proposed model without the consideration of the transverse shear deformations in the model formulation indicate slightly higher values than the frequencies from the proposed model with the consideration of the shear deformations. The ignorance of shear deformations across the thickness of a beam leads to over-estimation of natural frequencies. However, the proposed model with consideration of transverse shear deformations shows close agreements of the frequency values with reported data as shown in Fig. 4(a). These results show fewer deviations, around 2.22%, 5.56%, and 6.51%, respectively, for the first three flexural natural frequencies from the published results.

The validity of these results is also checked with the modal response obtained from the 3D FEM of the tapered composite beam in this work. A 3D FE model is developed by using the *Soild185* element in ANSYS (total no. of elements: 54720). The convergence of the 3D FE model is

checked. In the 3D FE model, eight plies are dropped at one step of the tapered zone, and in this way, three steps are modeled to obtain the effect of 24 dropped-out plies. This ply-dropping sequence is in line with the ply-drop configuration of "D type" as mentioned in [22]. The dropped-out plies in the tapered section are modeled as matrix-rich layers; the corresponding epoxy properties are taken from [22]. The fixed-free boundary condition is modeled by constraining one end of the beam in all degrees of freedom and keeping another end free. The comparison of natural frequencies from 3D FEM and proposed 1D FEM is presented in Fig. 4 (a) itself. It shows very good quantitative agreement between results, as the percentage deviation is within 7% for the first three flexural natural frequencies.

4.1.2 Validation for delaminated tapered beam model

After the validation of the proposed model for a healthy tapered composite beam, it is extended to investigate the influence of delamination damage. The combined effect of thickness tapering and delamination damage will show notable reductions in the natural frequencies of a tapered composite beam [49], [50]. For analyzing this delamination influence, the same tapered composite beam geometry, which was utilized earlier for healthy conditions, is considered, and its results are compared with the published natural frequency results reported in [22]. The tapered beam is analyzed for the clamped-free boundary condition. The full-width delamination is introduced partially across the length of the beam of size 40 mm. The delamination is present in the tapered zone, and it is extended towards the thin zone of a beam at the first interface from the top lamina. This delamination configuration is assumed, as mentioned in [22], for a direct comparison of the natural frequency results. The comparison of the first three flexural natural frequencies of a delaminated tapered composite beam with published results and 3D FEM results is shown in Fig.

4(b). For the delaminated beam, the natural frequencies from the proposed model considering and ignoring the shear effect are presented in Fig. 4(b) for comparison.

It is observed that the proposed model (with shear) gives minor deviations (below 7%) for the first three natural frequencies as compared to the frequency values reported in [22]. The 3D FE model is also developed for a delaminated composite tapered beam on ANSYS by following the same procedure as described for a healthy beam in earlier discussions. The interfacial delamination of size 40 mm along the full length of the tapered zone and extending towards the partial length of the thin zone is modeled in ANSYS by disconnecting the respective nodes in that location at the first interface from the top lamina. The 3D FEM results for the first three flexural natural frequencies indicate respectively 0.56%, 6.21%, and 5.13% deviations from the published results in [22]. This shows a very good agreement between the proposed 1D FE model and the developed 3D FE model for a delaminated beam as well. After this model validation, the stochastic dynamic analysis of composite tapered beams is carried out to address the stochasticity in natural frequencies due to uncertainties in material properties which will help to showcase more realistic dynamic behavior of tapered composite laminates.

4.2 Stochastic analysis of tapered composite beams

This sub-section presents the stochastic response for natural frequencies of tapered composite beams under the influence of material property uncertainties at various scales. The present work captures the scatter in the micromechanical properties, which include mass densities, elastic constants, Poisson's ratios, and volume fractions measured at constituent levels. The affected dynamic performance of the tapered composite beams due to these uncertainties is presented in the form of stochastic distributions of natural frequencies based on a probabilistic modeling approach. The stochastic natural frequency results are presented for various healthy and

delaminated tapered composite beam cases. In all the stochastic simulations considered in this work, a clamped-free boundary condition is implemented. The micro-mechanical properties of the tapered composite beam are considered as continuous uncertain variables. A scatter of 5% and a sample size of 1000 are assumed in all the stochastic simulation studies presented here. The mean values of uncertain material inputs at the micro-scale, which are assumed to be normally distributed, are mentioned in Table 2, and the geometry details of the beam are taken from Table 1 (Ghaffari *et al.*[22]). The choice of normal distribution fit for all the micro-properties of tapered composite beams is assumed by referring to probabilistic modeling approaches for composite laminates reported in [51], [52].

Table 2 Mean values of uncertain material properties

Uncertain material properties	Mean Value
Longitudinal modulus of fiber (E_{1f})	189 GPa
Transverse modulus of fiber (E_{2f})	30 GPa
Shear modulus of fiber(G_{12f})	120 GPa
Elastic modulus of matrix (E_m)	3.93 GPa
Shear modulus of matrix (G_m)	1.034 GPa
Poisson's ratio for fiber	0.3
Poisson's ratio for matrix	0.37
Mass density for fiber	1800 kg/m^3
Mass density for matrix	1100 kg/m^3
Fiber volume fraction	0.62

4.2.1 Stochastic dynamic response of healthy composite tapered beams

In this sub-section, the influence of uncertainties in the micromechanical properties of a healthy tapered composite beam on the first three flexural frequencies is addressed. The source-induced uncertainties are quantified by analyzing the stochastic distributions of natural frequency outputs

of the tapered composite beams. Hereafter, in this paper, the first, second, and third flexural natural frequencies are presented and abbreviated as FNF, SNF, and TNF, respectively.

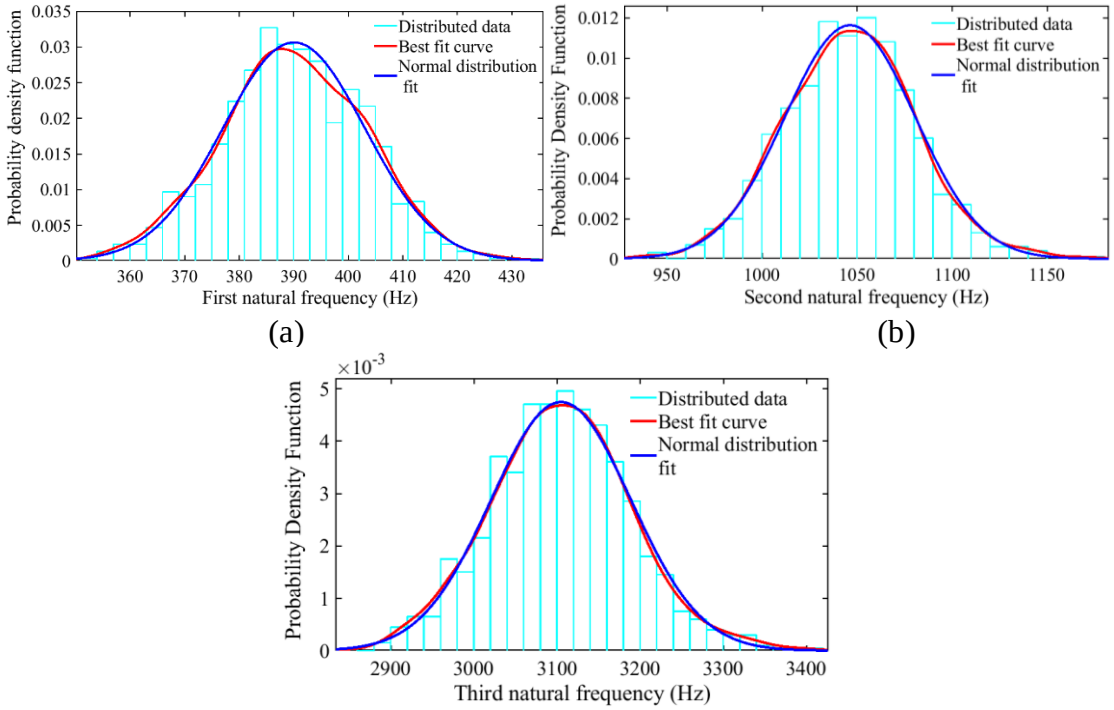

Fig. 5 Stochastic distribution of first three flexural natural frequencies of the tapered composite beam (a) FNF (389.90, 12.51) (b) SNF (1047.6,47.13) (c) TNF (3101.61,84.20)

In the caption of Fig. 5(a), Fig. 5(b), and Fig. 5(c), the first value mentioned in the bracket indicates the mean value, and the second indicates the standard deviation of PDF plots of natural frequencies The stochastic distribution data of the first three natural frequencies is shown in Fig. 5(a), 5(b), and 5(c), respectively, in histogram form. Also, the best-fit and normal-fit curves for this distributed data are indicated in the same Fig. 5 for the first three flexural natural frequencies. It is observed from Fig. 5(a), 5(b), and 5(c) that the normally distributed fit curve for the stochastic frequency data closely overlaps with the best-fit curve, which indicates the close matching of their statistical variables. To check the accuracy of the normal distribution fit to the distributed natural

frequency data, an estimation of the R-squared value for the fits of FNF, SNF, and TNF is carried out. It gives a value of 0.9015, 0.9040, and 0.8745 for FNF, SNF, and TNF, respectively. These values, which are close to 1 indicate betterness of the fits. It illustrates that FNF, SNF, and TNF are normally distributed.

The close observation of the PDF plots shown in Fig. 5(a), 5(b), and 5(c) indicate considerable reductions in PDF values corresponding to peak points of normally distributed PDF plots of SNF and TNF as compared to FNF. Further observation on the response bound indicates a 63.72% increase in the standard deviation of SNF distribution as compared to that of FNF. The same observation for the standard deviation values of TNF shows a 59 % increase as compared to SNF. The collective interpretation of these reported observations indicates the increased influence of uncertainties in material properties for higher modes which is reflected in the form of a wider spread of natural frequencies.

The influence of length ratio, which is measured by taking the ratio of the length of a thick section to the length of a thin section of a tapered composite beam, is found to be affecting the natural frequency distributions. Here the influence of three different length ratios of values 0.66, 1, and 1.5 on stochastic distributions of the first three flexural frequencies are analyzed and presented. Fig. 6 (a), 6(b), and 6(c), respectively, indicate the PDF plots of the first three flexural frequencies for different length ratios.

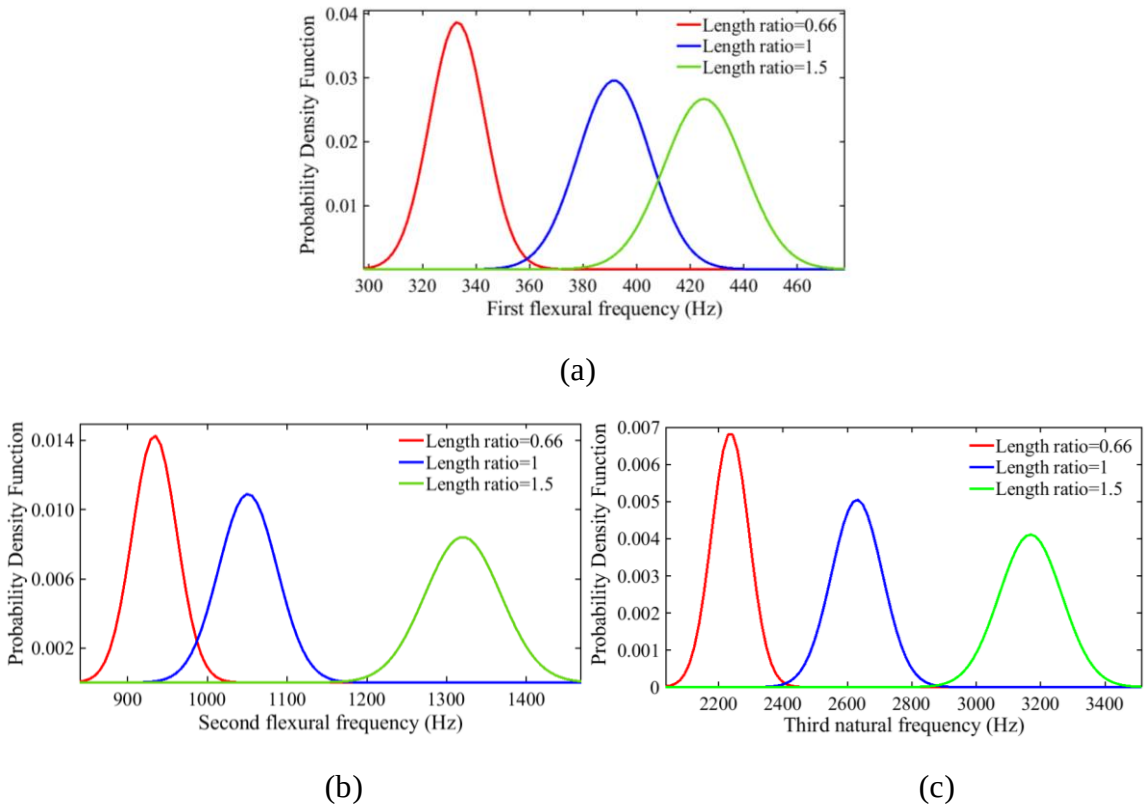

Fig. 6 Effect of length ratio on stochastic distribution of first three flexural natural frequencies (a) FNF (b) SNF (c) TNF

It is observed that for the increase in the length ratio of a tapered composite beam from 0.66 to 1.5, almost 21.47%, 29.45%, and 15.58% increments are reported in the mean frequencies of FNF, SNF, and TNF, respectively. Also, the response bound is found to be increased by almost 30-35%. This indicates that the uncertainties in material properties show a dominating influence for the tapered beams with higher length ratios due to observed wider response bounds.

Along with the length ratio, the thickness ratio is also an equally important geometrical parameter in the case of tapered composite beams. Fig. 7(a), 7(b), and 7(c), respectively, present the PDF plots for the first three flexural frequencies for three different thickness ratios. The thickness ratio of a tapered composite beam is defined as the ratio of the thickness of a thick section to the thickness of a thin section. It depends on the number of plies dropped in the tapered zone and

ultimately reflects the measure of the taper angle. Three thickness ratios of values 2,3, and 4 obtained due to dropping of 8,16, and 24 plies, respectively, are considered for the stochastic analysis. This consideration of thickness ratios is based on the correlation of taper angle with the no. of dropped-out plies mentioned in [13] for the composite tapered beam.

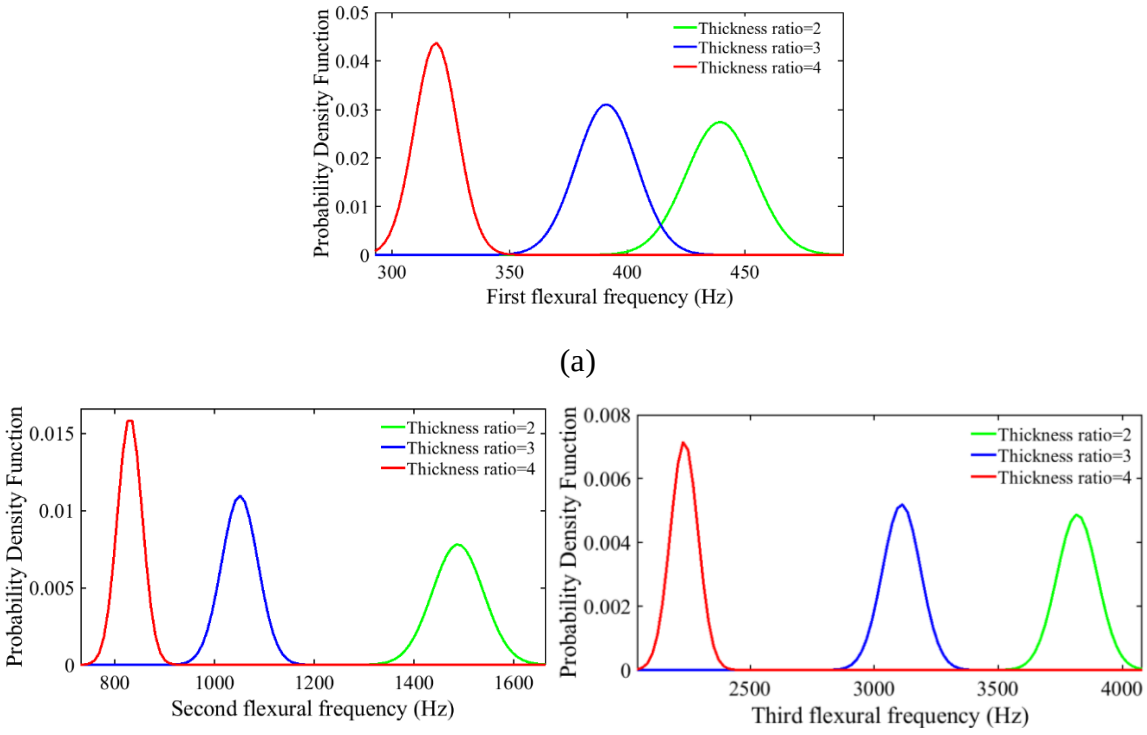

Fig. 7 Effect of thickness ratio on stochastic distribution of first three flexural frequencies (a) FNF (b) SNF (c) TNF

It is observed from PDF plots of the first three natural frequencies that, along with response bounds, PDF plots also indicate considerable reductions in mean values of natural frequencies for increased thickness ratios. From Fig. 7(a), it is calculated that the reduction in the response bound of FNF for an increased thickness ratio value from 2 to 3 is around 13.21%. Whereas this decrease in response bound of FNF for increased thickness ratio from 3 to 4 is almost 18%. The close observation of probability density function values of FNF, SNF, and TNF stochastic plots also indicates decrements in the values for decreased thickness ratios. These observations interpret that

the thickness ratio of tapered composite beams which signifies the tapered angle closely affects the stochastic distributions of natural frequencies as considerable changes in their statistical parameters are reported.

4.2.2 Stochastic response of a delaminated tapered composite beam

The stochastic natural frequencies of a tapered composite beam with embedded full width and partial length delamination introduced across the length of a beam of size 30 mm (almost 23% of total length) in the tapered zone are analyzed. The coupled influence of uncertainties in micro-properties and delamination damage conditions on stochastic natural frequencies of a composite tapered beam are presented in the form of PDF plots as shown in Fig. 8(a), 8(b), and 8(c) for the first three flexural frequencies respectively. The influence of extended delamination size of 23% of length in the thin zone of a beam, along with delamination presence in the tapered zone as well, is analyzed. The PDF plots of this larger delamination size of 46% of the length (23% in tapered zone +23% in thin zone) are also captured in the same Fig. 8.

The general observation from all the PDF plots presented for the first three flexural frequencies in Fig. 8(a), 8(b), and 8(c), respectively, is that, as the delamination size increases, there are decrements in the mean natural frequency values and the response bound of stochastic distributions of natural frequencies for a tapered composite beam. For the considered delamination configuration, the reduction in the mean value of FNF for a 23% delaminated beam is found to be almost 22.58% as compared to a healthy beam. The corresponding reduction in mean FNF for 46% delaminated beam as compared to that of 23% delaminated beam is found to be drastically lesser (almost 3.13%). For the case of 23% delamination, the mean value of SNF shows almost 11.37% reduction, and that of TNF shows a 15.26% reduction as compared to the healthy frequency values

as observed from Fig. 8(b) and 8(c), respectively. The trend of standard deviations of the PDF plots addressed in Fig. 8(a), 8(b), and 8(c) shows almost 35% reduction in the case of FNF, and 15-20% reductions are reported for SNF and TNF for delaminated beams as compared to healthy beams. These statistical observations demonstrate the dominance of delamination damage over uncertainties addressed at a micro level in which the delamination occurred in a tapered zone of a beam is a more sensitive location as that contributes more degradation in the natural frequencies.

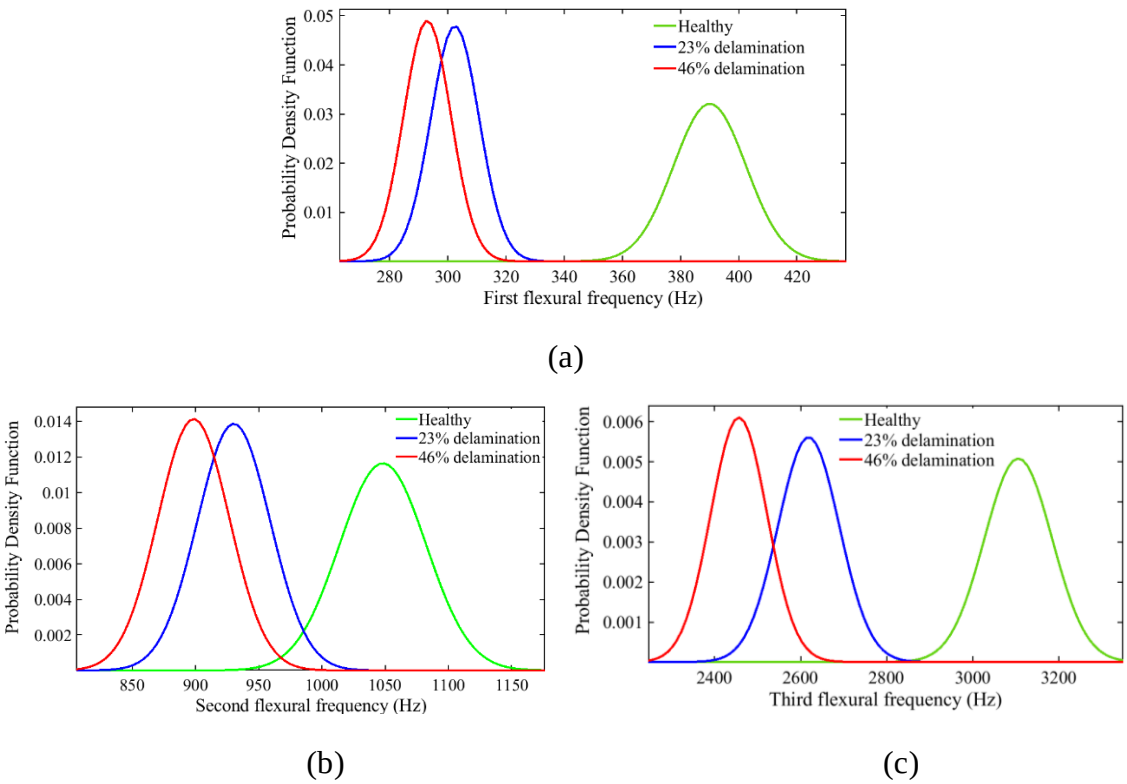

Fig. 8 PDF plots of first three flexural frequencies of a tapered beam with healthy and partially delaminated conditions (partial delamination sizes of 23% and 46% of length and full width) (a) FNF (b) SNF (c) TNF

An effect of the degree of stochasticity (DOS) which indicates the amount of scatter in the uncertain inputs on the stochastic distribution of the first flexural natural frequency for healthy and 23% delaminated cases are reported in Fig. 9(a) and 9(b) respectively in the form of PDF plots. A case of 23% delamination considered here represents the influence of delamination in the tapered

zone only. There are four simulations performed by varying the DOS percentage as: (i) case-1: DOS of 10% in micro-properties (ii) case-2: DOS of 20% in micro-properties (ii) case-3: DOS of 10% in macro-properties (iv) case-4: DOS of 20% in macro-properties.

4.2.3 Influence of degree of stochasticity in uncertain inputs on the stochastic natural frequency outputs of a healthy and delaminated tapered composite beam

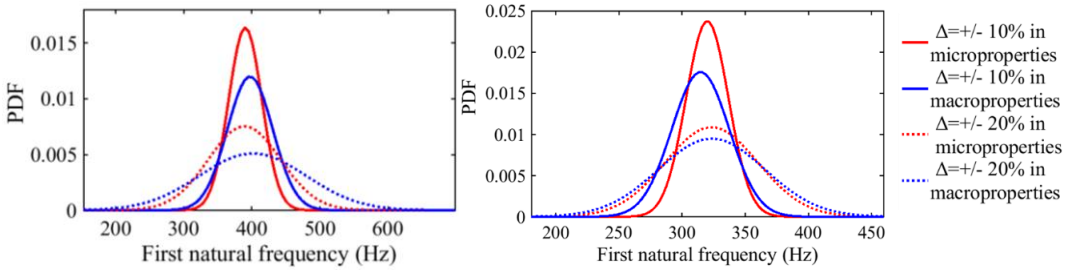

(a) (b)

Fig. 9 Effect of degree of stochasticity in micro and macro mechanical properties on PDF plots of first natural frequency (a) Healthy (b) 23% delamination in the tapered zone

It is observed from the PDF plots that as the DOS increases from 10% to 20%, there is an increase in the response bounds of the plots and a decrease in the probability density function values for all the DOS cases, as mentioned earlier. By analyzing the statistical parameters of the PDF plot for healthy beam case (Fig. 9(a)), almost 52% increment in the standard deviations and 50-55% decrease in the probability density function values are reported when DOS in micro-properties is changed from 10% to 20%. An increase in DOS of macro-properties from 10% to 20% reports almost a 48% increase in stochastic bounds of PDF plots and more than 40% decrease in probability density function values for the first flexural frequency distribution. These notable observations interpret that multi-scale uncertainties addressed at micro and macro scales strongly influence the stochastic distributions of natural frequencies.

The close observation of the statistical parameters of the PDF plot of the first natural frequency for the delaminated beam, as shown in Fig. 9(b), indicates more than 30% reductions in response bounds for all DOS cases as compared to response bounds observed for healthy beam in Fig. 9(a). Also, the probability density function values show more than 30% increments than that of healthy frequency distribution values. These accountable observations illustrate that the influence of delamination damage dominates over uncertainties in the material properties of the beam. This dominance is more pronounced here due to the more sensitive location of delamination in the tapered zone. A similar trend of the statistical parameters is observed for the second and third natural frequencies of healthy and delaminated tapered composite beams for all the DOS cases (Refer to Fig. S1 in the supplementary material). The influence of uncertainties is more pronounced for healthy beam cases. Hence, to understand the most dominating uncertain input that strongly affects the frequency distribution output, a sensitivity analysis is carried out for a healthy tapered composite beam.

4.3 Sensitivity analysis

The quantification of uncertainties is carried out in this subsection for a healthy beam case based on the sensitivity analysis studies. First, local sensitivity indices (LSI) are calculated by considering the variation of one uncertain parameter at a time. In the sensitivity analysis studies, the same composite tapered beam configuration is used as that mentioned in the previous section. Fig.10 (a) shows the LSI plot obtained for the first six modes of a tapered composite beam for various important uncertain variables. It is observed from Fig. 10(a) that the micro-scale uncertain variable of volume fraction and macro-scale variable of the mass density of lamina are highly sensitive which contributes to more variations in all the six natural frequencies of the first six modes. Fig. 10 (a) also indicates higher sensitivity of uncertain shear modulus of the matrix that

contributes to notable variation of torsional frequency (mode-4), whereas uncertainty in elastic modulus of the matrix shows higher sensitivity indices for initial bending and torsion modes (mode-1, 2, 3, 4). This discussion illustrates that the uncertainty in volume fractions, mass densities of a lamina, elastic modulus of the matrix, and shear modulus of the matrix are highly sensitive which contribute to more variations in the natural frequency outputs. Hence for further global sensitivity analysis (GSA) study, only these variables are taken into consideration.

The global sensitivity index (GSI) calculations are carried out as per the variance-based sensitivity analysis as mentioned in [53]. The most important advantage of GSA is that it addresses simultaneous variations in the uncertain parameters of the system [54]. A variance-based formulation for first and total order sensitivity indices is referred to from Ref. [55]. In the GSA, first, the sensitivities of fiber and matrix properties of a tapered composite beam are calculated based on a first-order sensitivity index plot as indicated in Fig. 10(b). This first-order sensitivity analysis is carried out by varying all fiber properties at a time and keeping all matrix properties constant in one iteration. Whereas, in another iteration, all fiber properties are kept constant, and all matrix properties are varied. Though it shows higher sensitivities of uncertain fiber properties over matrix properties, the SI values of uncertain matrix properties are also observed to be accountable from Fig. 10(b). This observation regarding matrix properties is obvious in the case of composite tapered beams because the dropped-out plies of the tapered beams are modeled by the matrix/resin layers.

The first-order and total-order GSI plots for four important uncertain variables obtained from earlier LSA are presented in Fig. 10(c) for the first flexural frequency. For the calculations of first and total order sensitivity indices, the variance-based formulation reported in [53] is referred. GSA plot of these variables interprets that the elastic modulus of the matrix is the most sensitive variable

as it gives higher first and total order indices indicating the higher fractional contribution of this variable towards variance in frequency outputs of the tapered composite beam. The uncertainty in the mass density of lamina also exhibits notable first and total order SI values indicating its higher sensitivity. However, the first and total order SI values of the variable volume fraction and shear modulus of the matrix are considerably lower. It indicates that these variables interact strongly with other uncertain variables and hence their individual uncertainty is less sensitive than their interacting capability with other uncertain parameters. The local and global sensitivity analysis results presented in this section help to understand the most important uncertain parameters from various scales of material properties of tapered composite beams which are dominantly responsible for stochastic variation in natural frequencies.

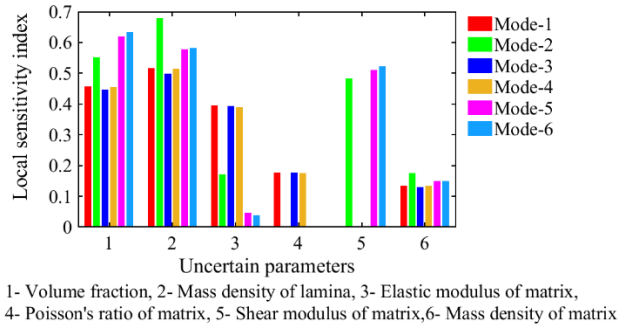

(a)

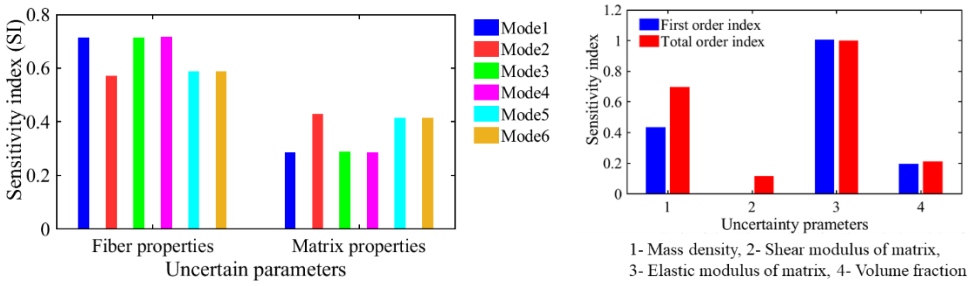

(b) (c)

Fig. 10 Sensitivity index plots of for tapered beam (a) local sensitivity index plot for individual uncertainty in various variables (b) RCOV values of uncertain fiber and uncertain matrix properties (c) Global sensitivity index plot for important uncertain variables

4.4 Implementation of the proposed model to realistic application: flexbeam structures

In this sub-section, additional dynamic analysis results are showcased for one of the actual applications of tapered composite beams as a flexbeam structure in a helicopter rotorcraft assembly. This realistic application is identified from the Ref. [1]. In this work, the authors have investigated interlaminar stresses at ply drop locations which eventually lead to potential sites of delamination occurrences. Hence, to dynamically analyze such a realistic example by the proposed model, the same flexbeam is considered to portray its deterministic and stochastic results of natural frequencies for healthy and delaminated conditions. The material and geometry details for this flexbeam are taken from [1] and are mentioned in Table 3 (Fish *et al.* [1]**)**. The cantilever boundary condition is assumed for the determination of natural frequencies.

Table 3 Material and geometry attributes of rotor hub flexbeams

Material property details		
Attribute	**Fish *et al.*** [1]	**Murri *et al.*** [56]
Longitudinal modulus (E_1)	44.1 GPa	131.1 GPa
Transverse modulus (E_2)	12.4 GPa	5.90 GPa
Poisson's ratio	0.28	0.361
In-plane shear modulus (G_{12})	4.48 GPa	4.24 GPa
Mass density	1600 kg/m^3	1480 kg/m^3
Geometrical attributes details		
Lay-up of thick section	$[0]_{28}$	$[0_9/(45/\text{-}45)_3/(45/\text{-}45)_2]_s$
Lay-up of thin section	$[0]_{16}$	$[0_9/(45/\text{-}45)_2]_s$
No. of dropped-out plies	12	12
Length of a beam (L)	184 mm	254 mm
Length of thick section	96.38 mm	84.66 mm
Length of thin section	61.33 mm	84.66 mm
Width (w)	21 mm	25.4 mm
Ply thickness (t_p)	0.216 mm	0.203 mm

The deterministic natural frequency results obtained from proposed 1D FE and 3D FE models for the first three flexural modes of healthy and delaminated flexbeams are tabulated in Table 4. For damaged conditions, an embedded, full-width delamination is assumed at the midplane of the

beam. Here, the midplane location is considered for delamination damage as it exhibits higher degradations in the cross-sectional stiffness matrix of composite laminates. Along the span, a partially introduced delamination of size 15% of the length of a beam is considered in the tapered zone. The ply drop sequence is modeled by referring to the "overlapped-dispersed" taper model configuration as mentioned in [1]. The proposed 1D FE model results are validated with the 3D FE model of the flexbeam developed in this work on ANSYS. The procedure of 3D model development is the same as that discussed in the previous sub-section 4.1.1 for another tapered beam configuration. The comparison of these results obtained for a healthy and 15% delaminated beam shows a very close agreement between the reduced 1D FE model values and the 3D FE model. The deviations between the 1D FE model and 3D FEM results are within 10% for the first three flexural natural frequencies of healthy as well as delaminated beams.

Table 4 Deterministic natural frequencies of first three flexural modes of rotor-hub flexbeam for healthy and delaminated conditions (flexbeam with 0^0 plies)

Frequency modes	Healthy beam-1D FEM	Healthy beam-3D FEM	15% delamination-1D FEM	15% delamination-3D FEM
Mode-1	258.24	237.39	227.72	225.15
Mode-2	1061.04	974.94	921.99	913.92
Mode-3	2846.84	2619.6	2439.29	2411

After observing accountable degradations in fundamental natural frequencies (around 12-15%) of a realistic delaminated flexbeam for a very small size delamination (15% of the length), the combined influence of delamination with associated source uncertainties of the flexbeam is analyzed. By referring to the sensitivity analysis results reported earlier in sub-section 4.3 for the composite tapered beam only those sensitive parameters are considered as uncertain inputs for the stochastic simulation of a flexbeam. These sensitive parameters are volume fraction (micro-scale), mass density (macro-scale), elastic modulus of matrix (micro-scale), and shear modulus of matrix

(micro-scale). A scatter of 10% is assumed in all these uncertain inputs, and stochastic distributions of the first three flexural frequencies are presented in the form of PDF plots in Fig. 11 (a), (b), and (c), respectively. In the stochastic simulation, an influence of increased delamination size, which is extended in a thin zone of the beam (30% and 45% of the spans), is also analyzed.

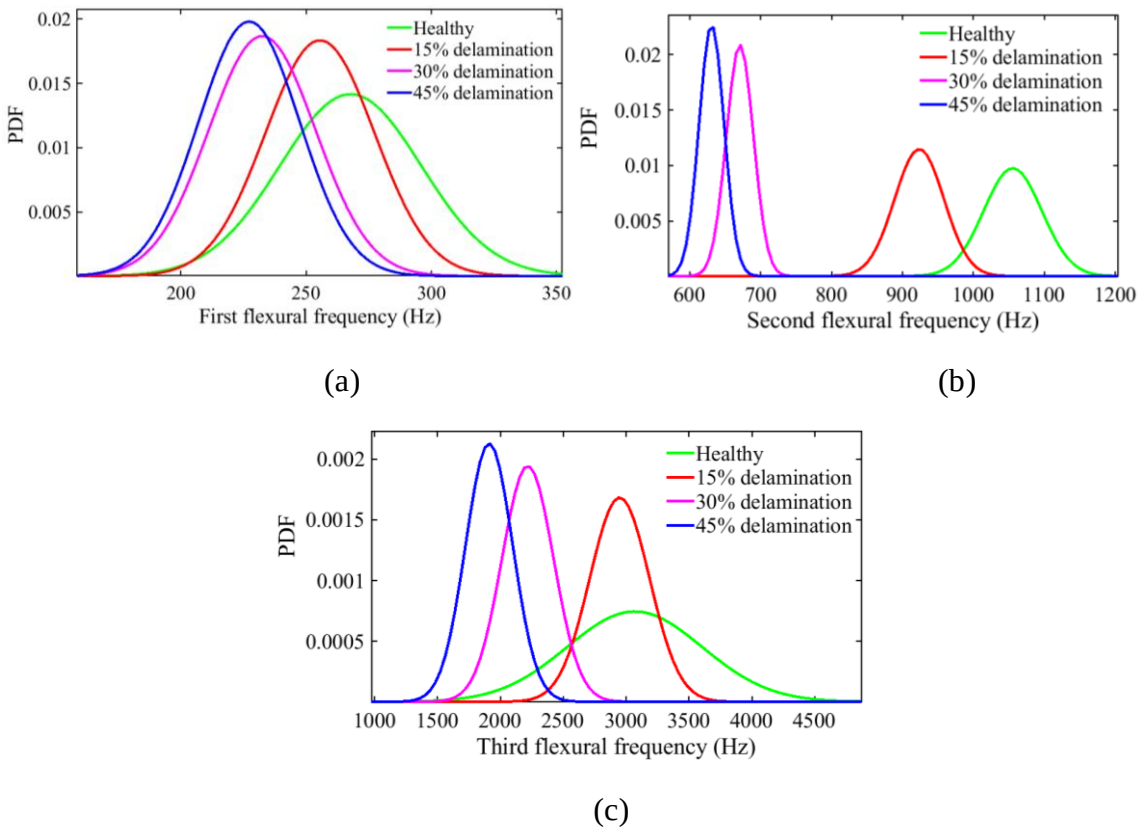

Fig. 11 Stochastic distributions of natural frequencies of a flexbeam example (a) first flexural mode, (b) second flexural mode, (c) third flexural mode

The observations of these stochastic results indicate comparatively higher degradations in mean natural frequencies of the second flexural mode, which is the major axis bending mode for the considered flexbeam as indicated in Fig. 11(b). This observation is obvious because a drastic reduction in major axis bending stiffness is reported as a result of the combined influence of the tapering effect and delamination damage degradation. The normalized stiffness degradation plots

for healthy and delaminated flexbeams are provided in the supplementary material (refer to Fig. S2 (a) and S2(b)). Fig. 11(a) and 11(c) represent the stochastic distributions of natural frequencies corresponding to minor axis bending. These two plots comparatively show lesser deviations in mean values and response bounds of natural frequencies for healthy and delaminated conditions of flexbeams.

Additionally, it is interesting to note from Fig. 11(a), 11(b), and 11(c) that the increase in the size of delamination in the thin zone minorly affects the stochastic distributions of natural frequencies. This observation is made by looking at very minor deviations in standard deviation and mean values for 30% and 45% delamination sizes.

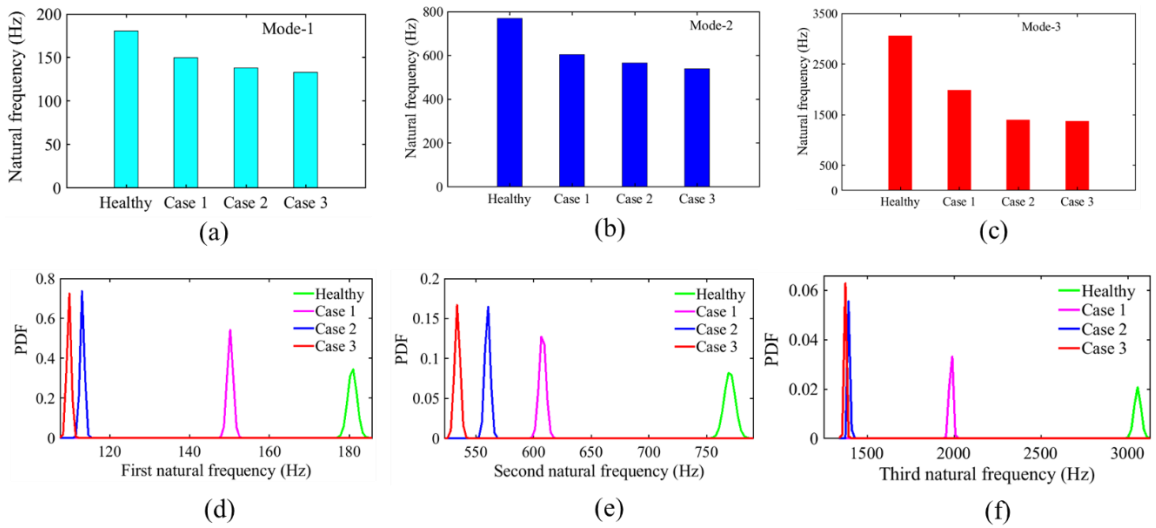

Fig. 12 Deterministic and stochastic natural frequency results of angle-ply flexbeam with healthy and delaminated configurations (a) mode 1 deterministic (b) mode 2 deterministic (c) mode 3 deterministic (d) stochastic frequency distribution mode 1 (e) stochastic frequency distribution mode 2 (f) stochastic frequency distribution mode 3

One more realistic application of the tapered composite beam reported in the literature as a rotor-hub flexbeam is addressed by Murri *et al.*[56]. The authors have tested the probable delamination sites in the case of tapered composite laminates of Graphite epoxy material with internal ply drops at NASA Langley Research Center. The same tapered composite beam configuration is considered

for dynamic analysis by implementing the VAM-based proposed model in this work. The reason for selecting this application of tapered composite beam lies in its specialized angle ply lay-up with 45^0 and -45^0 plies, and a group of 0^0 plies is present as a belt plies group. The geometry, lay-up, and material property details of this flexbeam are given in Table 3 (Murri *et al.* [56]). For the estimation of natural frequencies, a clamped-free boundary condition is considered.

The first three deterministic natural frequencies for healthy and delaminated configurations of the angle-ply flexbeam are presented in Fig. 12 (a), 12(b), and 12(c) respectively. In Fig. 12 (a), 12(b), and 12(c), cases 1, 2, 3 represent the delamination cases. Case-1 represents delamination in core plies of tapered zone, case-2 indicates delamination in a dropped ply and normal ply of the tapered zone, and case-3 shows delamination between two dropped plies of the tapered zone. These cases are taken concerning full-width embedded delamination introduced partially across the span of a beam. In all the cases, delamination is introduced between the 45^0 and -45^0 plies, and the partial delamination size across the beam span is 33.33% of the total length of the beam, which represents the occurrence of delamination in the tapered zone only.

It is observed from Fig. 12(a), 12(b), and 12(c) that up to 30% degradation in the natural frequencies of the first two modes and 48% degradation in the third frequency mode is reported for case-3 delamination (the delamination presence in core plies between 45^0 and -45^0 laminae). For case 2, where the delamination is present between one dropped and one normal ply, almost the same trend is observed in the degradation of the first three natural frequencies. Comparatively lesser but still notable degradations in the first three natural frequencies are observed for case-1, where delamination is introduced slightly away from the mid-plane and present between two dropped-out plies. The maximum degradation in the first three natural frequencies is observed for case-3 delamination as it is the location in the core plies close to the midplane. Third natural

frequencies for all delamination cases show the major degradation in the values (torsional mode of vibration). This is because the combined influence of delamination and tapering effect is found to degrade the torsional stiffness by almost 62% for case 3 delamination as compared to healthy and non-tapered sections. The same degradation in the flexural stiffness is found to be almost 54.16% for most sensitive case-3 delamination. This degradation in flexural stiffness is reflected in the decrements of the first two natural frequencies. The normalized degradation in torsional and flexural stiffness terms of the tapered zone section due to delamination is provided in Fig, S3 of the supplementary material.

To portray the more realistic natural frequency results of the angle-ply flexbeam, the influence of uncertainties in the macro-mechanical properties of the composite laminated flexbeam is analyzed for healthy and delaminated conditions of the beam. The scatter of 10% is assumed in the macro-properties of the ply, which include elastic modulus (E_1), transverse modulus (E_2), Poisson's ratio (ν_{12}), shear modulus (G_{12}), and mass density (ρ). The corresponding mean values of these macro-properties are taken from Table 3 (Murri *et al.* [56]), and all of them are assumed to be normally distributed. The stochastic natural frequency results for healthy and delaminated configurations (cases 1,2,3) are presented as PDF plots for the first three modes in Fig. 12 (d), 12(e), and 12(f). It is observed from stochastic distributions that the mean values and response bounds of the first three natural frequencies are drastically reduced for all delamination cases as compared to healthy cases. It is interesting here to address the stochastic frequency distribution for the torsional frequency mode (mode-3) which shows a dominant reduction in the mean frequency, response bound, and probability density function values (Fig. 12(f)). This notable stochastic frequency result for torsional frequency, which is highly influenced by material properties uncertainties and delamination conditions, is observed for this flexbeam application due to its specialized angle ply

lay-up. The consideration of delamination between 45^0 and -45^0 plies in all cases in the most sensitive tapered zone is also responsible for getting more degradations in the natural frequencies.

The results discussed highlight the measurable influence of uncertain material properties, delamination conditions, and lay-up on stochastic frequency distributions of healthy as well as delaminated angle-ply flexbeams. It also helps to highlight the more realistic dynamic response of the realistic applications of the tapered composite beams as flexbeams.

Stochastic analysis of systems, like structures with uncertain design variables, is computationally expensive. This is especially true if a traditional method like the Monte-Carlo (MC) method is used in the analysis. Although there are improvements to the MC method that can aid faster analysis, the problem is still computationally challenging due to the large number of simulations that must be repeated for the design variables. The stochastic analysis becomes doubly challenging if the underlying model used in the simulations is computationally demanding. A straightforward approach to alleviate this problem is to use a surrogate model in the simulations. However, predictions from surrogate models are questionable if an appropriate choice based on the mechanics of the problem is not made. For a problem with geometrical complexity like flexbeam having a number of design variables this is major challenge. To a large extent, a VAM based stochastic framework used in this work overcomes the challenges mentioned above.

A VAM based structural model is a reduced order model. For the flexbeam problem, the model gives exact analytical solution of the cross-sectional stiffness with the representation of all the design variables appearing in all the stiffness terms. This significantly reduces the computational time. Additionally, since it is an asymptotically correct reduced order model, the results closely mimick the simulation results from an explicit 3D numerical approach. The structural responses

are relatable to design variables, which may not be possible easily if the simulations are based on a direct 3D numerical approach, and lends naturally to linearization (following an order-based asymptotic approach), making it computationally economical. Please refer to Refs. [52], [57] that highlight the computational efficiency of a VAM-based stochastic analysis framework. On the contrary, extending the VAM-based approach to more complex geometrical configurations is difficult. For complex geometrical configurations, like strips/beams with airfoil shapes or other open or closed cross-sections, it is not possible to determine the cross-sectional stiffness terms analytically. One has to pursue either a semi-analytical or a numerical approach; however, the framework will still be computationally economical compared to a direct numerical approach, but interpreting the direct influence of design variables on the structural response is likely to be difficult. Finally, the current framework's efficacy is only demonstrated for investigating the linear dynamical behavior of a flexbeam. Its veracity to investigate the stochastic nonlinear dynamics of a flexbeam has yet to be explored in detail.

Conclusions

In this paper, the free vibration responses of healthy and delaminated tapered composite beams are analyzed by implementing a computationally accurate VAM framework coupled with a reduced 1D FE model. An asymptotically correct closed-form solution is derived for cross-sectional stiffness terms of healthy and delaminated tapered composite beams using the VAM framework. As delamination damage is observed most likely to occur in the case of tapered composite laminates, its combined influence with source uncertainties is analyzed in the form of stochastic frequency distributions. The deterministic and stochastic natural frequency results of the realistic applications of tapered composite beams as flexbeam structures in the helicopter rotor-blade assembly are presented and discussed. The concluding remarks are as follows:

1. The proposed VAM-based formulation can be applied to thin, or moderately thick sections of a tapered composite beam as it accounts for the transverse shear deformations in the formulation. The specialty of the proposed work lies in the development of a generalized five-layer cross-sectional stiffness model for the non-homogeneous tapered zone of a beam, which can be easily implemented in any ply drop configuration and delaminated sub-laminates.
2. The natural frequency results for healthy and delaminated configurations are strongly dependent on the lay-up of the beam. The full-width delamination in the lay-up with 0^0 plies of a flexbeam shows moderate reductions in flexural stiffness which is reflected in respective moderate degradation in major axis flexural frequency mode. But, in the case of angle-ply flexbeam with 45^0 and -45^0 plies in the lay-up, the full-width delamination introduced between 45^0 and -45^0 plies strongly degrades the torsional stiffness, followed by flexural stiffness terms. Hence, the natural frequencies of this flexbeam show drastic reductions in flexural as well as torsional frequency modes.
3. The global sensitivity results taken for quantification of uncertainties in micro-properties of the tapered composite beams exhibit the notable contributions of uncertainties in matrix properties in the variations of natural frequency outputs. The stochastic frequency distributions of tapered composite beams with healthy configuration show a more pronounced effect of source uncertainties addressed at the fiber and matrix level of the composite laminates. Whereas the respective stochastic frequency distributions for delaminated configuration show the dominance of delamination due to reported reductions in the response bounds as compared to healthy beams.

4. The stochastic frequency distributions for the extended delamination case in the thin zone from the tapered zone indicate maximum degradations in the mean frequency values for the delamination case introduced in the tapered zone of a beam. It indicates the tapered zone as the most sensitive delamination location.

The proposed results showcase the dynamic analysis response of more realistic composite structures by presenting the natural frequency results under more realistic conditions of uncertainties in the case of tapered composite laminates. Also, it accounts for the most probable damage sites of delamination especially pronounced in the case of tapered composite laminates due to termination of the plies.

Appendix

A_1- Cross-sectional stiffness terms of healthy, non-tapered cross-section (for thick/thin zones of tapered beam)

$$S_{11}^{nH} = \left(\frac{B\left(C_{13}^{2}C_{22} - 2C_{12}C_{13}C_{23} + C_{12}^{2}C_{33} + C_{11}\left(C_{23}^{2} - C_{22}C_{33}\right)\right)H}{C_{23}^{2} - C_{22}C_{33}} \right) \tag{A1}$$

$$S_{22}^{nH} = 2BC_{66}H$$

$$S_{33}^{nH} = 2\ \mathrm{B}\ \mathrm{C}_{55}\ \mathrm{H}$$

$$S_{44}^{nH} = BH^{3}\left(\frac{1}{3}C_{66}\right) + \frac{4\left(C_{66} - C_{55}\right)}{\pi^{4}}\left(\begin{array}{l} \mathrm{Sech}\left(\frac{B\pi}{2H}\right)^{2} + \frac{1}{81}\mathrm{Sech}\left(\frac{3B\pi}{2H}\right)^{2} + \\ \frac{1}{625}\mathrm{Sech}\left(\frac{5B\pi}{2H}\right)^{2} + \frac{1}{2401}\mathrm{Sech}\left(\frac{7B\pi}{2H}\right)^{2} \end{array} \right) + \ldots$$

$$\frac{H}{B}\frac{8\left(C_{55} - 7C_{66}\right)}{\pi^{5}}\left(\tanh\left(\frac{B\pi}{2H}\right) + \frac{1}{243}\tanh\left(\frac{3B\pi}{2H}\right) + \frac{1}{3125}\tanh\left(\frac{5B\pi}{2H}\right) + \frac{1}{16807}\tanh\left(\frac{7B\pi}{2H}\right)\right)$$

$$S_{55}^{nH} = \frac{B\left(C_{13}^{2}C_{22} - 2C_{12}C_{13}C_{23} + C_{12}^{2}C_{33} + C_{11}\left(C_{23}^{2} - C_{22}C_{33}\right)\right)H^{3}}{12\left(C_{23}^{2} - C_{22}C_{33}\right)}$$

$$S_{66}^{nH} = \frac{B^{3}\left(C_{13}^{2}C_{22} - C_{12}^{2}C_{33} + C_{11}\left(C_{23}^{2} - C_{22}C_{33}\right)\right)H}{12\left(C_{23}^{2} - C_{22}C_{33}\right)}$$

A_2- Cross-sectional stiffness terms of healthy, tapered cross-section (for the tapered zone of tapered beam carrying matrix-rich plies)

$$S_{11}^{mH} = B\left(\begin{array}{l} C_{11}\left(d_1 + d_2 + h\right) + \frac{BC_{13}^{2}C_{22}\left(d_1 + d_2 + h\right)}{C_{23}^{2} - C_{22}C_{33}} - \frac{2BC_{12}C_{13}C_{23}\left(d_1 + d_2 + h\right)}{C_{23}^{2} - C_{22}C_{33}} \\ - \frac{BC_{12}^{2}C_{33}\left(d_1 + d_2 + h\right)}{-C_{23}^{2} + C_{22}C_{33}} + Cr_{11}\left(\left(t_1 + t_2\right) + \frac{Cr_{12}^{2}\left(t_1 + t_2\right)}{\left(Cr_{11} + Cr_{12}\right)^{2}} - \frac{2Cr_{12}^{2}\left(t_1 + t_2\right)}{Cr_{11} + Cr_{12}} \right) \end{array} \right) \tag{A2}$$

$$S_{22}^{mH} = 2\left(BC_{66}\left(d_1 + d_2 + h\right) + \frac{2BCr_{11}\left(t_1 + t_2\right)}{3} \right)$$

$$S_{33}^{mH} = \frac{8BC_{55}Cr_{11}\left(d_1 + d_2 + h\right)}{2C_{55}h + Cr_{11}h} - \frac{4BC_{55}Cr_{11}\left(t_1 + t_2\right)t_1}{2C_{55}d_1 + Cr_{11}\left(d_1 + h\right)}$$

$$S_{44}^{mH} = \begin{pmatrix} \frac{1}{8}BC_{66}\left(d_1^{\,3} + d_2^{\,3} + h^3\right) + \frac{1}{8}BCr_{55}\left(t_1^{\,3} + t_2^{\,3}\right) + \ldots \\ \frac{1}{4}BC_{66}d_1^{\,2}t_1 + \frac{1}{4}BCr_{55}d_1^{\,2}t_1 + \frac{1}{4}BC_{66}d_2^{\,2}t_2 + \frac{1}{4}BCr_{55}d_2^{\,2}t_2 \end{pmatrix}$$

$$S_{55}^{mH} = \begin{pmatrix} \frac{1}{12}BC_{11} + \frac{1}{12}BCr_{11} + \frac{BC_{12}C_{13}C_{23}^{\,3}}{4\left(C_{23}^{\,2} - C_{22}C_{33}\right)^2} + \frac{BC_{13}^{\,2}C_{22}^{\,2}C_{33}}{4\left(C_{23}^{\,2} - C_{22}C_{33}\right)^2} + \\ \frac{BC_{12}^{\,2}C_{22}C_{33}^{\,2}}{12\left(C_{23}^{\,2} - C_{22}C_{33}\right)^2} + \frac{BC_{13}^{\,2}C_{22}C_{23}^{\,2}}{8\left(-C_{23}^{\,2} + C_{22}C_{33}\right)^2} + \frac{BC_{13}^{\,2}C_{22}^{\,2}C_{33}}{8\left(-C_{23}^{\,2} + C_{22}C_{33}\right)^2} \\ -\frac{BC_{12}C_{13}C_{22}C_{23}C_{33}}{6\left(-C_{23}^{\,2} + C_{22}C_{33}\right)^2} + \frac{BC_{12}^{\,2}C_{23}^{\,2}C_{33}}{8\left(-C_{23}^{\,2} + C_{22}C_{33}\right)^2} + \frac{BC_{12}^{\,2}C_{22}C_{33}^{\,2}}{8\left(-C_{23}^{\,2} + C_{22}C_{33}\right)^2} \end{pmatrix}\left(d_1^{\,3} + d_2^{\,3} + h^3\right)$$

$$+\left(\frac{BCr_{11}Cr_{12}^{\,2}}{12\left(Cr_{11} + Cr_{12}\right)^2} - \frac{BCr_{12}^{\,2}\left(t_1^{\,3} + t_2^{\,3}\right)}{6\left(Cr_{11} + Cr_{12}\right)} \right)\left(t_1^{\,3} + t_2^{\,3}\right)$$

$$S_{66}^{mH} = \frac{1}{12}B^3\left(d_1 + d_2 + h\right)\left(C_{11} + \frac{C_{13}^{\,2}C_{22}}{\left(C_{23}^{\,2} - C_{22}C_{33}\right)} - \frac{C_{12}C_{13}C_{23}}{\left(C_{23}^{\,2} - C_{22}C_{33}\right)} + \frac{C_{12}^{\,2}C_{33}}{\left(C_{23}^{\,2} - C_{22}C_{33}\right)} \right) +$$

$$\frac{1}{12}B^3\left(t_1 + t_2\right)\left(Cr_{11} + \frac{Cr_{11}Cr_{12}^{\,2}}{6\left(Cr_{11} + Cr_{12}\right)^2} - \frac{Cr12^2}{3\left(Cr_{11} + Cr_{12}\right)} + \frac{Cr_{12}^{\,2}Cr_{55}}{3\left(Cr_{11} + Cr_{12}\right)^2} \right)$$

$$S_{13}^{mH} = B\left(C_{11} + \frac{BC_{13}^{\,2}C_{22}}{\left(C_{23}^{\,2} - C_{22}C_{33}\right)} - \frac{2BC12C13C23}{\left(C_{23}^{\,2} - C_{22}C_{33}\right)} - \frac{BC12^2C33}{\left(-C_{23}^{\,2} + C_{22}C_{33}\right)} \right)\left(d_1 + d_2 + h\right)$$

A_3- Cross-sectional stiffness terms for the delaminated condition of tapered cross-section

(A3)

$$S_{11}^{mD}=\frac{1}{\left(\left(C_{23}^2-C_{22}C_{33}\right)\left(Cr_{11}+Cr_{12}\right)^2\right)}\begin{pmatrix}\begin{pmatrix}3C_{33}Cr_{11}^2\_2C_{23}^2Cr_{11}^3-2C_{22}C_{33}Cr_{11}^3+6C_{12}^2C_{33}Cr_{11}Cr_{12}-\\4C_{22}C_{33}Cr_{11}^2Cr_{12}+3C_{12}^2C_{33}Cr_{12}^2-4C_{23}^2Cr_{12}^3+4C_{22}C_{33}Cr_{12}^3+\\3C_{13}^2C_{22}\left(Cr_{11}+Cr_{12}\right)^2-6C_{12}C_{13}C_{23}\left(Cr_{11}+Cr_{12}\right)^2+\\3C_{11}\left(C_{23}^2-C_{22}C_{33}\right)\left(Cr_{11}+Cr_{12}\right)^2\end{pmatrix}\\\left(x_{2l}\left(x_{3b}-x_{3t}\right)+x_{2r}\left(-x_{3b}+x_{3t}\right)+\left(x_{2l2}-x_{2r2}\right)\left(x_{3b2}-x_{3t2}\right)\right)\end{pmatrix}$$

$$S_{22}^{mD}=4\left(3C_{66}+2Cr_{55}\right)\left(x_{2l}\left(x_{3b}-x_{3t}\right)+x_{2r}\left(-x_{3b}+x_{3t}\right)\right)+\left(x_{2l2}-x_{2r2}\right)\left(x_{3b2}-x_{3t2}\right)$$

$$S_{33}^{mD}=\frac{1}{\left(2C_{55}d_1+Cr_{11}(d_1+h)\right)^2\left(Cr_{11}(d_1+h)+2C_{55}t_1\right)^2}\begin{pmatrix}4C_{55}(3{Cr_{11}}^4(d_1+h)^2(d_1+h-t1)^2+48{C_{55}}^4{t_1}^2(d_1+t_1)^2+\\16{C_{55}}^3(2Cr_{55}{d_1}^2(d_1+h+t_1)^2+3Cr_{11}t_1(d_1+t_1)({d_1}^2+(2h-t_1)t_1+\\d_1(h+2t_1)))+4C_{55}{Cr_{11}}^2(d_1+h)(2Cr_{55}(d_1+h)(d1+h+t1)^2+\\3Cr_{11}({d_1}^3+{d_1}^2(2h+t_1)+d_1(h^2+3ht_1-3{t_1}^2)+t_1(2h^2-3ht_1+{t_1}^2)))\\+4{C_{55}}^2Cr_{11}(8Cr_{55}d_1(d_1+h)(d_1+h+t_1)^2+3Cr_{11}({d_1}^4+2{d_1}^3(h+3t_1)+\\2d_1t_1(3h^2+4ht_1-3{t_1}^2)+{t_1}^2(6h^2-6ht_1+{t_1}^2)+{d_1}^2(h^2+12ht_1+2{t_1}^2))\\(x_{2l}(x_{3b}-x_{3t})+x_{2r}(-x_{3b}+x_{3t})+(x_{2l2}-x_{2r2})(x_{3b}-x_{3t2}))\end{pmatrix}$$

$$S_{44}^{mD}=\frac{3}{4}C_{66}d_1^2x_{2l}x_{3b}+\frac{1}{2}Cr_{55}d_1^2x_{2l}x_{3b}+\frac{3}{2}C_{66}d_1t_1x_{2l}x_{3b}+Cr_{55}d_1t_1x_{2l}x_{3b}+\frac{3}{4}C_{66}t_1^2x_{2l}x_{3b}$$

$$S_{55}^{mD}=\frac{1}{(6({C_{23}}^2-C_{22}C_{33})(Cr_{11}+Cr_{12})^2)}\begin{pmatrix}6C_{12}C_{13}C_{23}(Cr_{11}+Cr_{12})^2(x_{2r}({x_{3b}}^3-{x_{3t}}^3)+x_{2l}(-{x_{3b}}^3+{x_{3t}}^3)-(x_{2l2}-x_{2r2})({x_{3b2}}^3-{x_{3t2}}^3))+\\3{C_{1\,2}}^2C_{33}(Cr_{11}+Cr_{12})^2(x_{2l}({x_{3b}}^3-{x_{3t}}^3)+x_{2r}(-{x_{3b}}^3+{x_{3t}}^3)+(x_{2l2}-x_{2r2})({x_{3b2}}^3-{x_{3t2}}^3))+\\{C_{23}}^2(4{Cr_{12}}^3(x_{2r}({x_{3b}}^3-{x_{3t}}^3)+x_{2l}(-{x_{3b}}^3+{x_{3t}}^3)-(x_{2l2}-x_{2r2})({x_{3b2}}^3-{x_{3t2}}^3)))+\\{Cr_{11}}^2(3C_{11}+2Cr_{11})(x_{2l}({x_{3b}}^3-{x_{3t}}^3)+x_{2r}(-{x_{3b}}^3+{x_{3t}}^3)+(x_{2l2}-x_{2r2})({x_{3b2}}^3-{x_{3t2}}^3))+\\2Cr_{11}(3C_{11}+2Cr_{11})Cr_{12}(x_{2l}({x_{3b}}^3-{x_{3t}}^3)++x_{2r}(-{x_{3b}}^3+{x_{3t}}^3)+(x_{2l2}-x_{2r2})\\({x_{3b2}}^3-{x_{3t2}}^3))+{Cr_{12}}^2(2Cr_{55}(x_{2l}{}^3(x_{3b}-x_{3t})+{x_{2r}}^3(-x_{3b}+x_{3t})+({x_{2l2}}^3-{x_{2r2}}^3)(x_{3b2}-x_{3t2}))+\\3C_{11}(x_{2l}({x_{3b}}^3-{x_{3t}}^3)+x_{2r}(-{x_{3b}}^3+{x_{3t}}^3)+(x_{2l2}-x_{2r2})({x_{3b2}}^3-{x_{3t2}}^3)))+C_{22}(3{C_{13}}^2(Cr_{11}+Cr_{12})^2\\(x_{2l}({x_{3b}}^3-{x_{3t}}^3)+x_{2r}(-{x_{3b}}^3+{x_{3t}}^3)+(x_{2l2}-x_{2r2})({x_{3b2}}^3-{x_{3t2}}^3))+{Cr_{12}}^2(-2Cr_{55}(x_{2l}{}^3(x_{3b}-x_{3t})+\\{x_{2r}}^3(-x_{3b}+x_{3t})+({x_{2l2}}^3-{x_{2r2}}^3)(x_{3b2}-x_{3t2}))+3C_{11}(x_{2r}({x_{3b}}^3-{x_{3t}}^3)+x_{2l}(-{x_{3b}}^3+{x_{3t}}^3)-\\(x_{2l2}-x_{2r2})({x_{3b2}}^3-{x_{3t2}}^3))\end{pmatrix}$$

$$S_{66}^{mD}=\frac{1}{6(C_{23}{}^{2}-C_{22}C_{33})(Cr_{11}+Cr_{12})^{2}}\begin{pmatrix}-3C_{12}{}^{2}C_{33}Cr_{11}{}^{2}x_{2l}{}^{3}x_{3b}-6C_{12}{}^{2}C_{33}Cr_{11}Cr_{12}x_{2l}{}^{3}x_{3b}+4C_{23}{}^{2}Cr_{11}{}^{2}Cr_{12}x_{2l}{}^{3}x_{3b}-4C_{22}C_{33}Cr_{11}{}^{2}Cr_{12}x_{2l}{}^{3}x_{3b}-\\3C_{12}{}^{2}C_{33}Cr_{12}{}^{2}x_{2l}{}^{3}x_{3b}+3C_{12}{}^{2}C_{33}Cr_{11}{}^{2}x_{2r}{}^{3}x_{3b}+6C_{12}{}^{2}C_{33}Cr_{11}Cr_{12}x_{2r}{}^{3}x_{3b}-4C_{23}{}^{2}Cr_{11}{}^{2}Cr_{12}x_{2r}{}^{3}x_{3b}+\\4C_{22}C_{33}Cr_{11}{}^{2}Cr_{12}x_{2r}{}^{3}x_{3b}+3C_{12}{}^{2}C_{33}Cr_{12}{}^{2}x_{2r}{}^{3}x_{3b}+4C_{23}{}^{2}Cr_{12}{}^{3}x_{2r}{}^{3}x_{3b}+8C_{23}{}^{2}Cr_{12}{}^{2}Cr_{55}x_{2l}x_{3b}{}^{3}-\\8C_{22}C_{33}Cr_{12}{}^{2}Cr_{55}x_{2l}x_{3b}{}^{3}-8C_{23}{}^{2}Cr_{12}Cr_{55}x_{2r}x_{3b}{}^{3}+8C_{22}C_{33}Cr_{12}{}^{2}Cr_{55}x_{2r}x_{3b}{}^{3}-3C_{12}{}^{2}C_{33}Cr_{11}{}^{2}x_{2l2}{}^{3}x_{3b2}-\\6C_{12}{}^{2}C_{33}Cr_{11}Cr_{12}x_{2l2}{}^{3}x_{3b2}+4C_{23}{}^{2}Cr_{11}{}^{2}Cr_{12}x_{2l2}{}^{3}x_{3b2}-4C_{22}C_{33}Cr_{11}{}^{2}Cr_{12}x_{2l2}{}^{3}x_{3b2}-3C_{12}{}^{2}C_{33}Cr_{12}{}^{2}x_{2l2}{}^{3}x_{3b2}+\\4C_{22}C_{33}Cr_{11}{}^{2}Cr_{12}x_{2l2}{}^{3}x_{3b2}-3C_{12}{}^{2}C_{33}Cr_{12}{}^{2}x_{2l2}{}^{3}x_{3b2}+4C_{22}C_{33}Cr_{11}{}^{2}Cr_{12}x_{2r2}{}^{3}x_{3b2}+3C_{12}{}^{2}C_{33}Cr_{12}{}^{2}x_{2r2}{}^{3}x_{3b2}+\\8C_{23}{}^{2}Cr_{12}{}^{2}Cr_{55}x_{2l2}x_{3b2}{}^{3}-8C_{22}C_{33}Cr_{12}{}^{2}Cr_{55}x_{2l2}x_{3b2}{}^{3}++3C_{12}{}^{2}C_{33}Cr_{11}{}^{2}x_{2l}{}^{3}x_{3t}-2C_{23}{}^{2}Cr_{11}{}^{3}x_{2l}{}^{3}x_{3t}+\\2C_{22}C_{33}Cr_{11}{}^{3}x_{2l}{}^{3}x_{3t}+6C_{12}{}^{2}C_{33}Cr_{11}Cr_{12}x_{2l}{}^{3}x_{3t}-4C_{23}{}^{2}Cr_{11}{}^{2}Cr_{12}x_{2l}{}^{3}x_{3t}+4C_{22}C_{33}Cr_{11}{}^{2}Cr_{12}x_{2l}{}^{3}x_{3t}+\\3C_{12}{}^{2}C_{33}Cr_{12}{}^{2}x_{2l}{}^{3}x_{3t}+4C_{23}{}^{2}Cr_{12}{}^{3}x_{2l}{}^{3}x_{3t}-4C_{22}C_{33}Cr_{12}{}^{3}x_{2l}{}^{3}x_{3t}-3C_{12}{}^{2}C_{33}Cr_{11}{}^{2}x_{2r}{}^{3}x_{3t}+2C_{23}{}^{2}Cr_{11}{}^{3}x_{2r}{}^{3}x_{3t}-\\2C_{22}C_{33}Cr_{11}{}^{3}x_{2r}{}^{3}x_{3t}-6C_{12}{}^{2}C_{33}Cr_{11}Cr_{12}x_{2r}{}^{3}x_{3t}+4C_{23}{}^{2}Cr_{11}{}^{2}Cr_{12}x_{2r}{}^{3}x_{3t}-4C_{22}C_{33}Cr_{11}{}^{2}Cr_{12}x_{2r}{}^{3}x_{3t}-\\3C_{12}{}^{2}C_{33}Cr_{12}{}^{2}x_{2r}{}^{3}x_{3t}-4C_{23}{}^{2}Cr_{12}{}^{3}x_{2r}{}^{3}x_{3t}+4C_{22}C_{33}Cr_{12}{}^{3}x_{2r}{}^{3}x_{3t}-8C_{23}{}^{2}Cr_{12}{}^{2}Cr_{55}x_{2l}x_{3t}{}^{3}+8C_{22}C_{33}Cr_{12}{}^{2}Cr_{55}x_{2l}x_{3t}{}^{3}+\\8C_{23}{}^{2}Cr_{12}{}^{2}Cr_{55}x_{2r}x_{3t}{}^{3}-8C_{22}C_{33}Cr_{12}{}^{2}Cr_{55}x_{2r}x_{3t}{}^{3}+2C_{23}{}^{2}Cr_{11}{}^{3}x_{2l2}{}^{3}x_{3t2}+2C_{22}C_{33}Cr_{11}{}^{3}x_{2l2}{}^{3}x_{3t2}+6C_{12}{}^{2}C_{33}Cr_{11}Cr_{12}x_{2l2}{}^{3}x_{3t2}-\\4C_{23}{}^{2}Cr_{11}{}^{2}Cr_{12}x_{2l2}{}^{3}x_{3t2}+4C_{22}C_{33}Cr_{11}{}^{2}Cr_{12}x_{2l2}{}^{3}x_{3t2}+3C_{12}{}^{2}C_{33}Cr_{12}{}^{2}x_{2l2}{}^{3}x_{3t2}\end{pmatrix}$$

A_4- Cross-sectional stiffness terms for the delaminated condition of non-tapered cross-sections (thick/thin zones)

$$S_{11}^{nD}=C_{11}\left(x_{2l}x_{3b}-x_{2r}x_{3b}-\frac{x_{2l}x_{3t}}{2}+\frac{x_{2r}x_{3t}}{2}\right)+C_{11}\left(x_{2l2}x_{3b2}-x_{2r2}x_{3b2}-\frac{x_{2l2}x_{3t2}}{2}+\frac{x_{2r2}x_{3t2}}{2}\right)+\frac{1}{(C_{23}{}^{2}-C_{22}C_{33})}$$
$$\begin{pmatrix}2C_{12}C_{13}C_{23}(x_{2l}-x_{2r})(-x_{3b}+x_{3t})+2C_{12}C_{13}C_{23}(x_{2l}-x_{2r})(-x_{3b}+x_{3t})+C_{13}{}^{2}C_{22}(x_{2l}-x_{2r})(-x_{3b}+x_{3t})+\\(C_{12}{}^{2}C_{33}(x_{2l}-x_{2r})(-x_{3b}+x_{3t})+C_{13}{}^{2}C_{22}(x_{2l2}-x_{2r2})(-x_{3b2}+x_{3t2})+C_{12}{}^{2}C_{33}(x_{2l2}-x_{2r2})(-x_{3b2}+x_{3t2})+\\(2C_{12}C_{13}C_{23}(x_{2l2}-x_{2r2})(-x_{3b2}+x_{3t2}))\end{pmatrix} \qquad (A_4)$$

$$S_{22}^{nD}=2\,C_{66}\,x_{2l}\,x_{3b}-2\,C_{66}\,x_{2r}\,x_{3b}+2\,C_{66}\,x_{2l2}\,x_{3b2}-2\,C_{66}\,x_{2r2}\,x_{3b2}-2\,C_{66}\,x_{2l}\,x_{3t}+2\,C_{66}\,x_{2r}\,x_{3t}-2\,C_{66}\,x_{2l2}\,x_{3t2}+2\,C_{66}\,x_{2r2}\,x_{3t2}$$

$$S_{33}^{nD}=2\,C_{55}\,x_{2l}\,x_{3b}-2\,C_{55}\,x_{2r}\,x_{3b}+2\,C_{55}\,x_{2l2}\,x_{3b2}-2\,C_{55}\,x_{2r2}\,x_{3b2}-2\,C_{55}\,x_{2l}\,x_{3t}+2\,C_{55}\,x_{2r}\,x_{3t}-2\,C_{55}\,x_{2l2}\,x_{3t2}+2\,C_{55}\,x_{2r2}\,x_{3t2}$$

$$S_{44}^{nD}=\frac{1}{6}\begin{pmatrix}C_{55}x_{2l}^{3}x_{3b}-C_{55}x_{2r}^{3}x_{3b}+C_{66}x_{2l}x_{3b}^{3}-C_{66}x_{2r}x_{3b}^{3}+C_{55}x_{2l2}{}^{3}x_{3b2}+C_{55}x_{2r2}{}^{3}x_{3b2}+C_{66}x_{2l2}x_{3b2}{}^{3}-\ldots\\C_{66}x_{2r2}x_{3b2}{}^{3}-C_{55}x_{2l}{}^{3}x_{3t}+C_{55}x_{2r}{}^{3}x_{3t}-C_{66}x_{2l}x_{3t}{}^{3}+C_{66}x_{2r}x_{3t}{}^{3}-C_{55}x_{2l2}{}^{3}x_{3t2}+C_{55}x_{2r2}{}^{3}x_{3t2}-\ldots\\C_{66}x_{2l2}x_{3t2}{}^{3}+C_{66}x_{2r2}x_{3t2}{}^{3}\end{pmatrix}$$

$$S_{24}^{nD}=-C_{66}x_{2l}x_{3b}{}^{2}+C_{66}x_{2r}x_{3b}{}^{2}-C_{66}x_{2l2}x_{3b2}{}^{2}+C_{66}x_{2r2}x_{3b2}{}^{2}+C_{66}x_{2l}x_{3t}{}^{2}-C_{66}x_{2r}x_{3t}{}^{2}$$

$$S_{55}^{nD}=\frac{1}{6}C_{11}\left(x_{2l}x_{3b}{}^{3}-x_{2r}x_{3b}{}^{3}+x_{2l2}x_{3b2}{}^{3}+x_{2r2}x_{3b2}{}^{3}+x_{2l}x_{3t}{}^{3}+x_{2r}x_{3t}{}^{3}-x_{2l2}x_{3t2}{}^{3}+x_{2r2}x_{3t2}{}^{3}\right)+\ldots$$
$$\frac{1}{3(C_{23}{}^{2}-C_{22}C_{33})}\left(2C_{12}C_{13}C_{23}(x_{2l}-x_{2r})(-x_{3b}{}^{3}+x_{3t}{}^{3})+2C_{12}C_{13}C_{23}(x_{2l2}-x_{2r2})(-x_{3b2}{}^{3}+x_{3t2}{}^{3})\right)$$

$$S66^{nD} = 2\left(\frac{1}{6}C_{11}\left({x_{2l}}^3 x_{3b} - {x_{2r}}^3 x_{3b} - {x_{2l}}^3 x_{3t} + {x_{2r}}^3 x_{3t}\right) + \frac{1}{3({C_{23}}^2 - C_{22}C_{33})}\begin{pmatrix} C_{12}C_{13}{C_{23}}^3({x_{2l}}^3 - {x_{2r}}^3)(x_{3b} - x_{3t}) + \\ {C_{13}}^2 C_{22}({x_{2l}}^3 - {x_{2r}}^3)(x_{3b} - x_{3t})) + \\ C_{12}C_{13}C_{23}({x_{2l}}^3 - {x_{2r}}^3)(-x_{3b} + x_{3t})) \end{pmatrix}\right) + \ldots$$

$$2\left(\frac{1}{6}C_{11}\left({x_{2l2}}^3 x_{3b2} - {x_{2r2}}^3 x_{3b2} - {x_{2l2}}^3 x_{3t2} + {x_{2r2}}^3 x_{3t2}\right) + \frac{1}{3({C_{23}}^2 - C_{22}C_{33})}\begin{pmatrix} C_{12}C_{13}{C_{23}}^3({x_{2l2}}^3 - {x_{2r2}}^3)(x_{3b2} - x_{3t2}) + \\ {C_{13}}^2 C_{22}({x_{2l2}}^3 - {x_{2r2}}^3)(x_{3b2} - x_{3t2})) + \\ C_{12}C_{13}C_{23}({x_{2l2}}^3 - {x_{2r2}}^3)(-x_{3b} + x_{3t})) \end{pmatrix}\right)$$

Note for delaminated stiffness terms in A_3 and A_4:
All the stiffness terms will be functions of width (B) and thickness (H) after putting appropriate limits for delamination size in x_2 and x_3 directions. For example, for full width delamination conditions, the limits of x_2 direction are taken as: $x_{2l}=x_{2l2}=-B/2$ and $x_{2r}=x_{2r2}=B/2$. Whereas for delamination at midplane of the stack condition, the limits of x_3 are taken as: $x_{3b}=x_{3b2}=-H/2$ and $x_{3t}=x_{3t2}=H/2$

Assumed zeroth order cross-sectional warping solutions for non-tapered cross-sections (thick/thin zones)

$$w_1[x_1,x_2,x_3] = \left(\frac{4H^2}{\pi^3}\begin{pmatrix} \operatorname{sech}\left(\frac{B\pi}{2H}\right)\sin\left(\frac{\pi x_3}{H}\right)\sinh\left(\frac{\pi x_2}{H}\right) - \frac{1}{27}\operatorname{sech}\left(\frac{3B\pi}{2H}\right)\sin\left(\frac{3\pi x_3}{H}\right)\sin\left(\frac{3\pi x_3}{H}\right) + \ldots \\ \frac{1}{125}\operatorname{sech}\left(\frac{5B\pi}{2H}\right)\sin\left(\frac{5\pi x_3}{H}\right)\sin\left(\frac{5\pi x_3}{H}\right) - \frac{1}{343}\operatorname{sech}\left(\frac{7B\pi}{2H}\right)\sin\left(\frac{7\pi x_3}{H}\right)\sin\left(\frac{7\pi x_3}{H}\right) \end{pmatrix} - x_2 x_3\right)k_1$$

$$w_2[x_1,x_2,x_3] = \frac{\left((C_{13}C_{22} - C_{13}C_{23})\left(H^2 - 12x_3^2\right)K_3 - \left(C_{13}C_{23} - C_{12}C_{33}\right)\left(-24x_2\left(\gamma_{11} + x_3K_2\right) - B^2K_3 + 12x_2^2K_3\right)\right)}{24\left(C_{22}C_{33} - C_{23}^2\right)} \qquad (A_5)$$

$$w_3[x_1,x_2,x_3] = \frac{\left((C_{13}C_{23} - C_{12}C_{33})\left(B^2 - 12x_2^2\right)K_2 - \left(C_{13}C_{22} - C_{12}C_{33}\right)\left(-24x_3\left(\gamma_{11} - x_2K_3\right) - H^2K_2 + 12x_3^2K_2\right)\right)}{24\left(C_{22}C_{33} - C_{23}^2\right)}$$

Assumed zeroth order cross-sectional warping solutions for tapered cross-sections

$$w_{1ni}[x_1,x_2,x_3] = \frac{-\left(2C_{55} - Cr_{11}\right)\left(2t_1^2 + t_1\left(x_{3t} - 2x_3\right)\right)\gamma_{13}}{Cr_{11}\left(d_1 + h\right) + 2C_{55}\left(x_{3b}\right)} + k_1\left(\begin{pmatrix} \frac{4d_1^2}{\pi^3}\operatorname{sech}\left(\frac{B\pi}{2d_1}\right)\sin\left(\frac{\pi x_3}{d_1}\right)\sinh\left(\frac{\pi x_2}{d_1}\right) - \\ \frac{1}{27}\operatorname{sech}\left(\frac{3B\pi}{2d_1}\right)\sin\left(\frac{3\pi x_3}{d_1}\right)\sinh\left(\frac{3\pi x_2}{d_1}\right) + \\ \frac{1}{125}\operatorname{sech}\left(\frac{5B\pi}{2d_1}\right)\sin\left(\frac{5\pi x_3}{d_1}\right)\sinh\left(\frac{5\pi x_2}{d_1}\right) \end{pmatrix} - \left(\frac{1}{2}x_2\left(-d_1 - t_1 + 2x_3\right)k_1\right)\right) \qquad (A_6)$$

$$w_{1mi}[x_1,x_2,x_3]=\frac{-(2C_{55}-Cr_{11})\left(2t_1^2+t_1(x_{3t}-2x_3)\right)\gamma_{11}}{Cr_{11}(d_1+h)+2C_{55}(x_{3b})}+k_1\left(\begin{array}{l}\frac{4t_1^2}{\pi^3}\operatorname{sech}\left(\frac{B\pi}{2t_1}\right)\sin\left(\frac{\pi x_3}{t_1}\right)\sinh\left(\frac{\pi x_2}{t_1}\right)-\\ \frac{1}{27}\operatorname{sech}\left(\frac{3B\pi}{2t_1}\right)\sin\left(\frac{3\pi x_3}{t_1}\right)\sinh\left(\frac{3\pi x_2}{t_1}\right)+\\ \frac{1}{125}\operatorname{sech}\left(\frac{5B\pi}{2t_1}\right)\sin\left(\frac{5\pi x_3}{t_1}\right)\sinh\left(\frac{5\pi x_2}{t_1}\right)\end{array}\right)-\left(\frac{1}{2}x_2(-d_1-t_1+2x_3)k_1\right)$$

$$w_{2ni}[x_1,x_2,x_3]=\frac{1}{24\left(-C_{23}^2+C_{22}C_{33}\right)}\left(\begin{array}{l}B^2(C_{13}C_{23}-C_{12}C_{33})K_3+4\left(\begin{array}{l}C_{13}C_{23}K_3x_2^2\left(3x_3^2-x_{3b}^2+x_{3b}x_{3t}-x_{3t}^2\right)+\\ C_{13}C_{23}K_3\left(-3x_3^2+x_{3b}^2-x_{3b}x_{3t}+x_{3t}^2\right)\end{array}\right)+\\ 3C_{13}C_{23}K_2\left(-K_3x_2+2\left(K_2x_3+\gamma_{11}\right)\right)\end{array}\right)$$

$$w_{2mi}[x_1,x_2,x_3]=\frac{-\left(Cr_{12}K_3\left(B^2+12x_3^2-4x_{3b}^2+4x_{3b}x_{3t}-4x_{3t}^2\right)\right)}{24(Cr_{11}+Cr_{12})}$$

$$w_{3ni}[x_1,x_2,x_3]=\frac{1}{24\left(-C_{23}^2+C_{22}C_{33}\right)}\left(B^2(C_{13}C_{23}-C_{12}C_{33})K_2+4\left(\begin{array}{l}-3C_{13}C_{23}K_2x_2^2+3C_{12}C_{33}K_2x_2^2+C_{13}C_{22}(6K_3x_2x_3)+\\ K_2\left(\left(-3x_3^2+x_{3b}^2-x_{3b}x_{3t}+x_{3t}^2\right)+3(-2x_3+x_{3b}+x_{3t})\right)\gamma_{11}-\\ -C_{12}C_{23}(6K_3x_2x_3)+K_2\left(\begin{array}{l}\left(-3x_3^2+x_{3b}^2-x_{3b}x_{3t}+x_{3t}^2\right)+\\ 3(-2x_3+x_{3b}+x_{3t})\end{array}\right)\gamma_{11}\end{array}\right)\right)$$

$$w_{3mi}[x_1,x_2,x_3]=\frac{Cr_{12}}{24(Cr_{11}+Cr_{12})}\left(-B^2K_2+4\left(6K_3x_2x_3+K_2\left(3x_2^2-3x_3^2+x_{3b}^2+x_{3b}x_{3t}+x_{3t}^2\right)\right)\right)$$

Here the notations w_{ini} and w_{imi} (i=1,2,3) are utilized to represent the warping solution for non-matrix-rich and matrix-rich layers respectively present in the tapered zone of a beam. The notations x_{3t} and x_{3b} represent the position of the considered layer/layers from mid-plane where suffix letters *t* and *b* represent the top and bottom positions of a layer or group of layers from mid-plane.

Acknowledgment

Priyanka Patil is grateful to her parent institute K. J. Somaiya College of Engineering, Mumbai for sponsoring her to pursue a doctoral program at IIT Bombay.

ORCID iDs

S Naskar: https://orcid.org/0000-0003-3294-8333

Priyanka Patil: https://orcid.org/0009-0009-1187-3644

Data availability statement

The datasets generated during and/or analyzed during the current study are available from the corresponding authors upon reasonable request.

Referances

[1] J. C. Fish and A. J. Vizzini, "Tailoring concepts for improved structural performance of rotorcraft flexbeams," *Compos. Eng.*, vol. 2, no. 5–7, pp. 303–312, 1992, doi: 10.1016/0961-9526(92)90028-5.

[2] W. Zhang, Y. Niu, and K. Behdinan, "Vibration characteristics of rotating pretwisted composite tapered blade with graphene coating layers," *Aerosp. Sci. Technol.*, vol. 98, p. 105644, 2020, doi: 10.1016/j.ast.2019.105644.

[3] S. Seraj and R. Ganesan, "Dynamic instability of rotating doubly-tapered laminated composite beams under periodic rotational speeds," *Compos. Struct.*, vol. 200, no. October 2017, pp. 711–728, 2018, doi: 10.1016/j.compstruct.2018.05.133.

[4] H. Prahlad and I. Chopra, "Development of an adaptive flexbeam for rotorcraft applications using embedded Shape Memory Alloy (SMA) actuators," *Collect. Tech. Pap. - AIAA/ASME/ASCE/AHS/ASC Struct. Struct. Dyn. Mater. Conf.*, vol. 2, pp. 248–261, 2000, doi: 10.2514/6.2000-1712.

[5] K. C. Kim, "Dynamic analysis of bearingless main rotor (BMR) system with hub flexbeam damage," *Collect. Tech. Pap. - AIAA/ASME/ASCE/AHS/ASC Struct. Struct. Dyn. Mater. Conf.*, vol. 4, no. April, pp. 2208–2216, 1995, doi: 10.2514/6.1995-1149.

[6] S. N. Jung, K. T. Kim, and S. J. Kim, "Aeroelastic stability analysis of hingeless rotor blade with composite flexures," *Collect. Tech. Pap. - AIAA/ASME/ASCE/AHS/ASC Struct. Struct. Dyn. Mater. Conf.*, vol. 1, pp. 897–905, 1997, doi: 10.2514/6.1997-1285.

[7] L. S. Raju, G. V. Rao, and K. K. Raju, "Large amplitude free vibrations of tapered beams," *AIAA J.*, vol. 14, no. 2, pp. 280–282, 1976, doi: 10.2514/3.7095.

[8] C. B. Smith and M. Wereley, "Active-passive constrained layer damping of composite rotating flexbeams," *AIAA/ASME/AHS Adapt. Struct. Forum, 1996*, pp. 207–216, 1996, doi: 10.2514/6.1996-1290.

[9] S. Ramalingerswara Rao and N. Ganesan, "Dynamic response of tapered composite beams using higher order shear deformation theory," *J. Sound Vib.*, vol. 187, no. 5, pp. 737–756, 1995, doi: 10.1006/jsvi.1995.0560.

[10] S. Ramalingeswara Rao and N. Ganesan, "Dynamic response of non-uniform composite beams," *J. Sound Vib.*, vol. 200, no. 5, pp. 563–577, 1997, doi: 10.1006/jsvi.1995.9987.

[11] R. S. Gupta and S. S. Rao, “Finite element eigenvalue analysis of tapered and twisted Timoshenko beams,” *J. Sound Vib.*, vol. 56, no. 2, pp. 187–200, 1978, doi: 10.1016/S0022-460X(78)80014-5.

[12] X. Tong, B. Tabarrok, and K. Y. Yeh, “Vibration analysis of timoshenko beams with non-homogeneity and varying cross-section,” *J. Sound Vib.*, vol. 186, no. 5, pp. 821–835, 1995, doi: 10.1006/jsvi.1995.0490.

[13] A. Zabihollah, “Vibration and Buckling Analyes of Tapered Composite Beams Using Conventional and Advanced Finite Element Formulations.” p. 260, 2003.

[14] B. C. Lin, T. F. Xie, M. Xu, Y. H. Li, and J. Yang, “Natural frequencies and dynamic responses of rotating composite non-uniform beams with an elastically root in hygrothermal environment,” *Compos. Struct.*, vol. 209, no. September 2018, pp. 968–980, 2019, doi: 10.1016/j.compstruct.2018.11.029.

[15] A. Fazili and R. Ganesan, “Natural Frequencies Of Internally-Doubly-Tapered Laminated Composite Beams,” pp. 1–7, 2018, doi: 10.25071/10315/35393.

[16] M. A. Fazili, “Vibration Analysis of Thickness- and Width- Tapered Laminated Composite Beams using Hierarchical Finite Element Method,” no. September, 2013.

[17] R. Ganesan and A. Zabihollah, “Vibration analysis of tapered composite beams using a higher-order finite element. Part II: parametric study,” *Compos. Struct.*, vol. 77, no. 3, pp. 319–330, 2007, doi: 10.1016/j.compstruct.2005.07.017.

[18] R. Ganesan and A. Zabihollah, “Vibration analysis of tapered composite beams using a higher-order finite element. Part I: Formulation,” *Compos. Struct.*, vol. 77, no. 3, pp. 306–318, 2007, doi: 10.1016/j.compstruct.2005.07.018.

[19] A. B. Arumugam, V. Rajamohan, A. Pandey, and P. E. Sudhagar, “Finite element vibration analysis of rotating laminated composite beam with varying cross-section using HSDT,” *Int. J. Interact. Des. Manuf.*, vol. 11, no. 3, pp. 703–712, 2017, doi: 10.1007/s12008-016-0364-x.

[20] A. Zak, M. Krawczuk, and W. Ostachowicz, “Numerical and experimental investigation of free vibration of multilayer delaminated composite beams and plates,” vol. 26, 2000.

[21] T. Mukhopadhyay, S. Naskar, P. K. Karsh, S. Dey, and Z. You, “E ff ect of delamination on the stochastic natural frequencies of composite laminates,” *Compos. Part B*, vol. 154, no. March, pp. 242–256, 2018, doi: 10.1016/j.compositesb.2018.07.029.

[22] H. Ghaffari, E. Saeedi, A. Zabihollah, and R. Ahmadi, “Vibration based damage detection in smart non-uniform thickness laminated composite beams,” *TIC-STH’09 2009 IEEE Toronto Int. Conf. - Sci. Technol. Humanit.*, pp. 176–181, 2009, doi: 10.1109/TIC-STH.2009.5444512.

[23] V. Moorthy and K. Marappan, “Identification of delamination severity in a tapered FRP composite plate,” *Compos. Struct.*, vol. 299, no. August, p. 116054, 2022, doi: 10.1016/j.compstruct.2022.116054.

[24] N. Grover, R. Sahoo, B. N. Singh, and D. K. Maiti, “Influence of parametric uncertainties on the deflection statistics of general laminated composite and sandwich plates,” *Compos. Struct.*, vol. 171, pp. 158–169, 2017, doi: 10.1016/j.compstruct.2017.03.036.

[25] S. Sriramula and M. K. Chryssanthopoulos, “Quantification of uncertainty modelling in stochastic analysis of FRP composites,” *Composites Part A: Applied Science and Manufacturing*, vol. 40, no. 11. pp. 1673–1684, Nov. 2009. doi: 10.1016/j.compositesa.2009.08.020.

[26] M. A. Elseifi, M. R. Khalessi, H. Z. Lin, G. Rogers, and T. Y. Torng, “Probabilistic analysis of thick composite plates with manufacturing and material uncertainties,” *19th AIAA Appl. Aerodyn. Conf.*, no. c, 2001, doi: 10.2514/6.2001-1612.

[27] M. Fakoor and H. Parviz, “Uncertainty propagation in dynamics of composite plates: A semi-analytical non-sampling-based approach,” *Front. Struct. Civ. Eng.*, vol. 14, no. 6, pp. 1359–1371, 2020, doi: 10.1007/s11709-020-0658-8.

[28] X. Liang, H. Ning, D. Sun, and N. Hu, “Uncertainty analysis based on reduced-order models for composite structures with interval field variables,” *Compos. Struct.*, vol. 300, no. March, p. 116153, 2022, doi: 10.1016/j.compstruct.2022.116153.

[29] K. Sepahvand and S. Marburg, “Identification of composite uncertain material parameters from experimental modal data,” *Probabilistic Eng. Mech.*, vol. 37, pp. 148–153, 2014, doi: 10.1016/j.probengmech.2014.06.008.

[30] S. Naskar, “Susmita Naskar Aberdeen , United Kingdom,” no. January, 2019, doi: 10.13140/RG.2.2.17696.84483.

[31] S. Naskar, T. Mukhopadhyay, S. Sriramula, and S. Adhikari, “Stochastic natural frequency analysis of damaged thin-walled laminated composite beams with uncertainty in micromechanical properties,” *Compos. Struct.*, vol. 160, pp. 312–334, 2017, doi: 10.1016/j.compstruct.2016.10.035.

[32] T. Mukhopadhyay, S. Naskar, S. Dey, and S. Adhikari, “On quantifying the effect of noise in surrogate based stochastic free vibration analysis of laminated composite shallow shells,” *Compos. Struct.*, vol. 140, pp. 798–805, 2016, doi: 10.1016/j.compstruct.2015.12.037.

[33] T. Mukhopadhyay, S. Naskar, S. Chakraborty, P. K. Karsh, R. Choudhury, and S. Dey, “Stochastic Oblique Impact on Composite Laminates: A Concise Review and Characterization of the Essence of Hybrid Machine Learning Algorithms,” *Arch. Comput. Methods Eng.*, vol. 28, no. 3, pp. 1731–1760, 2021, doi: 10.1007/s11831-020-09438-w.

[34] S. Naskar, T. Mukhopadhyay, and S. Sriramula, “Probabilistic micromechanical spatial variability quanti fi cation in laminated composites,” *Compos. Part B*, vol. 151, no. May, pp. 291–325, 2018, doi: 10.1016/j.compositesb.2018.06.002.

[35] H. An, B. D. Youn, and H. S. Kim, “Reliability-based Design Optimization of Laminated Composite Structures under Delamination and Material Property Uncertainties,” *Int. J.*

Mech. Sci., vol. 205, no. May, p. 106561, 2021, doi: 10.1016/j.ijmecsci.2021.106561.

[36] A. Shaw, S. Sriramula, P. D. Gosling, and M. K. Chryssanthopoulos, "Composites : Part B A critical reliability evaluation of fibre reinforced composite materials based on probabilistic micro and macro-mechanical analysis," *Compos. Part B*, vol. 41, no. 6, pp. 446–453, 2010, doi: 10.1016/j.compositesb.2010.05.005.

[37] D. H. Oh and L. Librescu, "Free vibration and reliability of composite cantilevers featuring uncertain properties," *Reliab. Eng. Syst. Saf.*, vol. 56, no. 3, pp. 265–272, 1997, doi: 10.1016/S0951-8320(96)00038-5.

[38] X. Y. Zhou, S. Y. Qian, N. W. Wang, W. Xiong, and W. Q. Wu, "A review on stochastic multiscale analysis for FRP composite structures," *Compos. Struct.*, vol. 284, no. October 2021, 2022, doi: 10.1016/j.compstruct.2021.115132.

[39] Vaishali, T. Mukhopadhyay, S. Naskar, and S. Dey, "On machine learning assisted data-driven bridging of FSDT and HOZT for high-fidelity uncertainty quantification of laminated composite and sandwich plates," *Compos. Struct.*, vol. 304, no. P1, p. 116276, 2023, doi: 10.1016/j.compstruct.2022.116276.

[40] F. Kamali and F. Shahabian, "Free Vibration of Axially Functionally Graded Tapered Micro-Beams Considering Uncertain Properties," vol. 5, no. 4, pp. 543–556, 2022, doi: 10.22060/ajce.2022.18056.5657.

[41] N. Thi, T. Duy, N. Van Thuan, and D. Ngoc, "Stochastic finite element analysis of the free vibration of non-uniform beams with uncertain material," vol. 9, pp. 29–37, 2022.

[42] M. Kara, A. Seçgin, T. Baygün, and Ç. G. Akyol, "Stochastic prediction of natural frequencies of laminated composite beams by using a high-order statistical moment based approach," *Compos. Struct.*, vol. 290, no. December 2021, 2022, doi: 10.1016/j.compstruct.2022.115562.

[43] P. J. Guruprasad, M. Thejasvi, and D. Harursampath, "Nonlinear analysis of a thin pre-twisted and delaminated anisotropic strip," *Acta Mech.*, vol. 225, no. 10, pp. 2815–2832, 2014, doi: 10.1007/s00707-014-1203-4.

[44] S. B. Salunkhe, C. V Singh, and P. J. Guruprasad, "Effect of matrix cracks and delamination on extension-twist coupling of thin pretwisted composite strips," vol. 180, pp. 234–250, 2017, doi: 10.1016/j.compstruct.2017.07.072.

[45] P. Prakasha, M. Mitra, and P. J. Guruprasad, "Wave propagation in thin pretwisted composite strips with an embedded delamination," *J. Sound Vib.*, vol. 551, no. December 2022, p. 117600, 2023, doi: 10.1016/j.jsv.2023.117600.

[46] D. H. Hodges, D. Harursampath, V. V. Volovoi, and C. E. S. Cesnik, "Non-classical effects in non-linear analysis of pretwisted anisotropic strips," *Int. J. Non. Linear. Mech.*, vol. 34, no. 2, pp. 259–277, 1999, doi: 10.1016/S0020-7462(98)00023-7.

[47] P. Patil, S. Naskar, and P. J. Guruprasad, "Multi-scale stochastic dynamic analysis of a damaged pretwisted composite strip," vol. 0, no. 0, pp. 1–26, 2024, doi:

10.1177/00219983241297095.

[48] P. M. Mujumdar and S. Suryanarayan, “Flexural vibrations of beams with delaminations,” *J. Sound Vib.*, vol. 125, no. 3, pp. 441–461, 1988, doi: 10.1016/0022-460X(88)90253-2.

[49] M. Almuslmani and R. Ganesan, “Vibration of tapered composite driveshaft based on the hierarchical finite element analysis,” *Compos. Struct.*, vol. 209, no. September 2018, pp. 905–927, 2019, doi: 10.1016/j.compstruct.2018.10.053.

[50] C. N. Della, “Vibration of Delaminated Composite Laminates : A Review,” vol. 60, no. January, pp. 1–20, 2007, doi: 10.1115/1.2375141.

[51] M. C. Shiao and C. C. Chamis, “Probabilistic evaluation of fuselage-type composite structures,” *Probabilistic Eng. Mech.*, vol. 14, no. 1–2, pp. 179–187, 1999, doi: 10.1016/s0266-8920(98)00027-7.

[52] P. Pitchai, N. Kumar, R. G. Nair, and P. J. Guruprasad, “A coupled framework of variational asymptotic method based homogenization technique and Monte Carlo approach for the uncertainty and sensitivity analysis of unidirectional composites,” *Compos. Struct.*, vol. 263, no. January, p. 113656, 2021, doi: 10.1016/j.compstruct.2021.113656.

[53] A. Saltelli, P. Annoni, I. Azzini, F. Campolongo, M. Ratto, and S. Tarantola, “Variance based sensitivity analysis of model output . Design and estimator for the total sensitivity index,” *Comput. Phys. Commun.*, vol. 181, no. 2, pp. 259–270, 2010, doi: 10.1016/j.cpc.2009.09.018.

[54] X. Y. Zhang, M. N. Trame, L. J. Lesko, and S. Schmidt, “Sobol sensitivity analysis: A tool to guide the development and evaluation of systems pharmacology models,” *CPT Pharmacometrics Syst. Pharmacol.*, vol. 4, no. 2, pp. 69–79, 2015, doi: 10.1002/psp4.6.

[55] W. Yun, Z. Lu, and X. Jiang, “An efficient sampling approach for variance-based sensitivity analysis based on the law of total variance in the successive intervals without overlapping,” *Mech. Syst. Signal Process.*, vol. 106, pp. 495–510, 2018, doi: 10.1016/j.ymssp.2018.01.015.

[56] G. B. Murri, T. K. O’Brien, and S. A. Salpekar, “Tension fatigue of glass/epoxy and graphite/epoxy tapered laminates,” *Annu. Forum Proc. - Am. Helicopter Soc.*, vol. 1, pp. 721–734, 1990.

[57] P. Pitchai, D. Harursampath, and P. J. Guruprasad, “Stochastic analysis of a three phase composite using variational asymptotic based homogenization technique coupled with stochastic reduced order model,” *Compos. Struct.*, vol. 316, no. October 2022, p. 117040, 2023, doi: 10.1016/j.compstruct.2023.117040.